Opening Mechanism of a Cyclic Nucleotide–gated Channel Based on Analysis of Single Channels Locked in Each Liganded State

MariaLuisa Ruiz and Jeffrey W. Karpen

From the Department of Physiology and Biophysics, University of Colorado School of Medicine, Denver, Colorado 80262

ABSTRACT   Cyclic nucleotide–gated channels contain four subunits, each with a binding site for cGMP or cAMP in the cytoplasmic COOH-terminal domain. Previous studies of the kinetic mechanism of activation have been hampered by the complication that ligands are continuously binding and unbinding at each of these sites. Thus, even at the single channel level, it has been difficult to distinguish changes in behavior that arise from a channel with a fixed number of ligands bound from those that occur upon the binding and unbinding of ligands. For example, it is often assumed that complex behaviors like multiple conductance levels and bursting occur only as a consequence of changes in the number of bound ligands. We have overcome these ambiguities by covalently tethering one ligand at a time to single rod cyclic nucleotide–gated channels (Ruiz, ML., and J.W. Karpen. 1997. *Nature*. 389:389–392). We find that with a fixed number of ligands locked in place the channel freely moves between three conductance states and undergoes bursting behavior. Furthermore, a thorough kinetic analysis of channels locked in doubly, triply, and fully liganded states reveals more than one kinetically distinguishable state at each conductance level. Thus, even when the channel contains a fixed number of bound ligands, it can assume at least nine distinct states. Such complex behavior is inconsistent with simple concerted or sequential allosteric models. The data at each level of liganding can be successfully described by the same connected state model (with different rate constants), suggesting that the channel undergoes the same set of conformational changes regardless of the number of bound ligands. A general allosteric model, which postulates one conformational change per subunit in both the absence and presence of ligand, comes close to providing enough kinetically distinct states. We propose an extension of this model, in which more than one conformational change per subunit can occur during the process of channel activation.

KEY WORDS: allosteric proteins • ligand-gated ion channels • photoaffinity labeling • patch clamp • retinal rod photoreceptors

introduction

Cyclic nucleotide-gated (CNG)[1] channels form a unique family of ion channels that are activated by the binding of cGMP or cAMP (reviewed in Finn et al., 1996). These channels are thought to be formed by the association of four subunits (Liu et al., 1996; Varnum and Zagotta, 1996), each containing a COOH-terminal binding site for ligand (Kaupp et al., 1989; Brown et al., 1995). In retinal photoreceptors and olfactory receptor neurons, two types of subunits (α and β) coassemble to form heteromultimeric channels (Kaupp et al., 1989; Dhallan et al., 1990; Chen et al., 1993; Bradley et al., 1994; Liman and Buck, 1994; Körschen et al., 1995; Biel et al., 1996). Activation of these channels is allosteric in nature, thus the binding of several cyclic nucleo-

tide molecules to the cytoplasmic binding domains induces conformational changes that cause the channel pore to open (Fesenko et al., 1985; Haynes et al., 1986; Zimmerman and Baylor, 1986; Nakamura and Gold, 1987; Karpen et al., 1988; reviewed in Zimmerman, 1995). CNG ion channels are excellent proteins in which to study allosteric activation because the binding sites for cGMP are readily accessible in excised inside-out patches, conformational changes induced by ligand binding can be observed in a single protein molecule in real time, and there is no detectable desensitization in the continued presence of ligand.

Although structure–function studies are beginning to shed light on which parts of the protein are involved in activation (e.g., Goulding et al., 1994; Liu et al., 1994; Gordon and Zagotta, 1995a; Varnum et al., 1995; Bucossi et al., 1997; Gordon et al., 1997; Tibbs et al., 1997; Varnum and Zagotta, 1997; Brown et al., 1998; Zong et al., 1998), the sequence of events leading to channel opening remains largely unclear. A complete kinetic model is required to piece together the structural changes that occur. Various allosteric models have been proposed that can fit dose–response data. How-

Address correspondence to Dr. Jeffrey W. Karpen, Department of Physiology and Biophysics, Campus Box C240, University of Colorado School of Medicine, 4200 East Ninth Avenue, Denver, CO 80262. Fax: 303-315-8110; E-mail: jeffrey.karpen@uchsc.edu

[1]*Abbreviations used in this paper:* APT, 8-*p*-azidophenacylthio; CNG channel, cyclic nucleotide–gated channel; KNF, Koshland-Nemethy-Filmer; MWC, Monod-Wyman-Changeux.

ever, as demonstrated for other allosteric proteins, equilibrium or steady state data are not sufficient to support one model to the exclusion of others. Even when kinetic transitions are studied at the single channel level, the constant binding and unbinding of cyclic nucleotides makes it difficult to correlate any particular event to a specific number of ligands bound. As a result, the intermediate states of activation, in particular, are poorly understood. Hence, previously proposed mechanisms tend to be oversimplified due to the limitations of the assays.

We have shown previously that these problems can be circumvented by locking single channels into each possible liganded state (Ruiz and Karpen, 1997) with the use of a photoaffinity analogue of cGMP, 8-*p*-azidophenacylthio-cGMP (APT-cGMP; Brown et al., 1993; Karpen and Brown, 1996). Two criteria were used to establish the number of ligands covalently attached to each channel. First, dose–response relations for free cGMP were measured before and after covalent attachment of ligand. Four discrete shifts from the control relation were observed corresponding to the attachment of one to four ligands. These shifted relations reflected graded changes in both the Hill coefficient and the effective concentration of cGMP ($K_{1/2}$). Second, the liganding assignments were supported by the obvious changes in opening behavior. It was then possible to accumulate minutes of data at each level of liganding, resulting in sufficient representation of all conformational states. We found that the channel locked in a certain liganded state could assume multiple conductance states. In other words, although ligands were fixed in their binding sites, the channel was not frozen into a single conformation, or conducting state. This was the key observation that allowed us to rule out the simple concerted allosteric model Monod-Wyman-Changeux (MWC; Monod et al., 1965) and the sequential model Koshland-Nemethy-Filmer (KNF; Koshland et al., 1966).

Recently, a complementary approach for determining the contribution of individual binding events to activation of CNG channels was described by Liu et al. (1998). Multiple binding site mutations were made that apparently destroy binding to the retinal channel subunit. Heteromeric channels were expressed in *Xenopus* oocytes by coinjecting RNA for this binding site–deficient subunit with RNA coding for an "intact" retinal subunit, in which the pore sequence was replaced by that from the higher conducting catfish olfactory channel. Single channel patches were then isolated and the unaltered binding sites in each channel were saturated with cGMP. Since the higher conducting pore region accompanied each unmutated binding site, different levels of conductance reported different numbers of active binding sites present in each channel. The findings in this study agree with our previous results that

there is significant opening in partially liganded channels. However, there are discrepancies in the degree of opening for some of the liganded states. These differences are discussed below.

The major purpose of this paper is to present the first kinetic analysis of a CNG channel in every liganded state. Surprisingly, at each level of liganding, as many as five closed states were revealed, and each conducting state exhibited transient and sustained conformations. This information provides further evidence against the simple, limiting mechanisms mentioned above, and allows us to propose a more complete model that describes the opening process of the retinal rod cGMP-gated channel.

materials and methods

Electrophysiology

Xenopus laevis oocytes were injected with cRNA encoding the α subunit of the bovine retinal rod cGMP-gated channel. After 3–5 d of incubation at 15°C, single channels were isolated in excised inside-out membrane patches. Electrodes were coated with Sylgard and resistances varied from 15 to 20 MΩ. All patches were studied in symmetrical control solution containing (mM): 130 NaCl, 2 HEPES, 0.02 EDTA, 1 EGTA, pH 7.6 with NaOH. For recording, channels were held at ±50 mV for at least 10 s, and switched to 0 mV for at least 15 s in between. Multiple segments at +50 mV were recorded under each condition so that at least 30 s of channel activity was used for all analyses. For dose–response assays, cGMP was added to the control solution. Patches that contained single channels were identified by the lack of multiple openings stacked on top of each other at high concentrations of cGMP. Although at low concentrations step-wise openings between subconducting levels were observed, single transitions from closed to fully open and vice versa occurred much more frequently than would be expected if the larger openings arose from multiple low conductance channels. The procedure at saturating cGMP normally took about 5 min, which has been shown to be a sufficient period of time to avoid spontaneous shifts in $K_{1/2}$ (Molokanova et al., 1997). Furthermore, during dose–response assays, most concentrations were checked at least twice. After each channel was subjected to a dose–response assay, a nearly saturating concentration (20 μM) of APT-cGMP (see Scheme I; Brown et al., 1993; Karpen and Brown, 1996; Ruiz and Karpen, 1997) was perfused onto the patch, and UV light (360 nm) was shone for timed periods (10–180 s) (Scheme I).

8-*p*-azidophenacylthio-cGMP (APT-cGMP)

(scheme i)
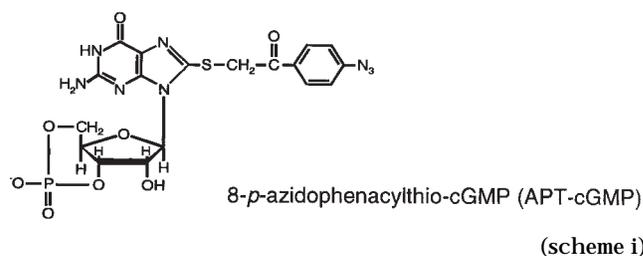
APT-cGMP binds to the channel's binding pockets and, upon UV photolysis, covalently attaches to the channel. In this way, cGMP becomes "locked" into the binding sites (Brown et al., 1993, 1995; Karpen and Brown, 1996; Ruiz and Karpen, 1997).

After UV exposure, patches were washed with control solution for at least 20 min to remove completely all unattached nucleotides from the patch (Karpen and Brown, 1996). After this treatment, behavior of partially liganded channels was recorded in control solution in the absence of free cGMP. Finally, a second dose–response assay was performed that proved to be shifted from the first if covalent attachment of ligand had occurred. It should be noted that UV exposure alone did not produce any shifts in the dose–response relation: in three patches, the relations were identical before and after typical exposure times. The number of ligands attached to individual channels was determined by the change in the slope of the dose–response relation (Hill coefficient) and by the change in behavior of the partially liganded channel in the absence of free ligand (see Ruiz and Karpen, 1997). Sometimes the channel entered into long closed states on the order of several hundreds of milliseconds, some as long as tens of seconds (Matthews and Watanabe, 1988; Nizzari et al., 1993; Taylor and Baylor, 1995). Since these sojourns were infrequent, we did not acquire enough events to analyze them adequately. However, they could be easily distinguished from "normal" channel activity with the use of stability plots (Colquhoun and Sigworth, 1995), and were excluded from the analyses. Single channel data were filtered at 50 kHz with a four-pole Bessel filter in the patch-clamp amplifier (Axopatch 200A; Axon Instruments), subsequently filtered at 5 kHz with an eight-pole Bessel filter, digitized at 88 kHz (Neuro-corder DR-484 PCM unit; Neuro Data Instruments), and stored on VHS tape. For most analyses, data were played back, filtered at 1 kHz (eight-pole Bessel filter), and sampled at 5 kHz. In some cases, the data were filtered at 5 kHz and sampled at 25 kHz. One record (from a triply liganded channel) was later digitally filtered at 500 Hz for compiling events.

Data Analysis

Each opening or closing event was idealized by simultaneously measuring the amplitude and dwell time (Pclamp6; Axon Instruments). Events were comprised of consecutive sample points that occurred within a single conductance class. The amplitudes of the sample points were averaged and the durations were summed to give the mean amplitude and dwell time of an idealized event. When a sample point fell into a different conductance class, a new event began. For identifying the conductance class of each event, three mean current amplitudes were typically set with horizontal lines at 0 (baseline), 0.3–0.4 (O1), 0.7–0.9 (O2), and 1.2-1.4 (O3) pA. These ranges reflect patch-to-patch variations; there were no systematic differences in current amplitudes between locked channels and channels activated by free ligand. Thresholds fell half way between the horizontal lines that defined the conductance classes. At a bandwidth of 1 kHz, events <0.6 ms were marked as "short" events with uncertain amplitudes (Pclamp6). The baseline was adjusted when it varied by more than ±0.015 pA for more than a few milliseconds. Once the event was accepted, its average amplitude and dwell time were added to the events list, and the conductance class was recorded. Noise and artifacts were excluded by eye during this process. After compiling the events list, dwell times were converted into probabilities (event time/total record time) for plotting against amplitudes in the amplitude histograms. The entire events list was binned for the amplitude histogram, including the short events. I/I_{max} was calculated as the mean current divided by the maximum current measured at saturating cGMP, on the same patch.

Conductance states were plotted separately for dwell-time fitting. Distributions were plotted as the square root of the normalized observations against the $\log_{10}$ of the dwell times (Sigworth and Sine, 1987). All distributions were fit with the maximum likelihood method. The "goodness of fit" for multiple components was determined by fitting a distribution with different numbers of components. The extent to which the addition of a component improved the fit was evaluated by the log-likelihood ratio test (Pclamp6). The rise-time of the filter (T_r) was 0.34 ms at 1 kHz, calculated as described (Howe et al., 1991; Colquhoun and Sigworth, 1995). Dwell times <2 T_r (0.6 ms) were not included in the exponential fits. The amplitude of the baseline noise at 1 kHz was typically ±0.1–0.15 pA about the mean, with a standard deviation (root mean square) of 0.02–0.03 pA (the false event detection rate was 1.6×10^{-19} s^{-1}). No corrections were made for missed events. However, the number of components in a fit are usually not affected by missed event errors, although the time constants may be somewhat overestimated (Colquhoun and Sigworth, 1995). The distributions provide only a lower bound for the number of states. In addition, errors arising from missed events are not nearly as severe when multiple thresholds are employed (Colquhoun and Hawkes, 1995).

Adjacent events were analyzed to determine the connections between states. The resolution of fast events was limited by the cutoff frequency of the filter. Thus, fast events classified as O1 or O2 might actually be O3 or closed events that were cut off during the rise time of the filter. This was handled at several different steps in the analysis. For adjacent state analysis, transitional events (on a rising or falling phase) less than T_r were combined with the following event. Peaks that were too brief to ascertain an amplitude were not removed initially, because they marked an interruption in an opening or closing event. Next, adjacent events were grouped by current amplitude (e.g., closed-O1 pairs would comprise one group). The first events in the pair were then sorted into kinetic classes based on the time constants and areas of the exponential fits. Subsequently, the second events were sorted into kinetic classes; again, the approximate number of events was dictated by the areas of the exponential fits. To rule out uncertain openings or closings, all open events shorter than 2 T_r were thrown out. The resolution of closings could be more precise ($>T_r$) because any event with an amplitude lower than 2 SD below the O1 state must be a closed event (Howe et al., 1991). Thus, only reliable events were used to determine the number of observed adjacent events for each kinetic class. When one connection occurred more often than any other, it was taken as a direct connection (see APPENDIX). These results were supported by component dependency calculations (Magleby and Song, 1992). In brief, component dependency is the percentage of observations that one state, i (which for simplicity is defined as one exponential component), was followed by another state, j, compared with the independent probability that those two states would occur adjacent to each other. This is calculated as follows: for any two states, i and j,

$$\text{component dependency} = [\text{Obs}(ij) - \text{Ex}(ij)]/\text{Ex}(ij),$$

where Obs(ij) is the observed number of adjacent events for states i and j, and Ex(ij) is the expected number of adjacent events that would be observed if the two events occurred independently of one another. Ex(ij) is the product of the probabilities that the two events could occur individually:

$$\text{Ex}(ij) = P_i^* P_j^* \text{ total number of events,}$$

where P_i and P_j are the individual probabilities:

$$P_i = (\text{total number of events in state } i)/ \\ (\text{total number of events in all states}),$$

and

$$P_j = (\text{total number of events in state } j)/ \\ (\text{total number of events in all states}).$$

Simulations

For simulations of the connected state models, the rate constants between each pair of connected states were put into a matrix format. As an initial screen for candidate models, steady state occupancies and mean currents were computed as described (Colquhoun and Hawkes, 1995) in order to predict the I/I_{max} value (mean current/maximum current). For further testing, current traces were simulated by starting at the longest closed state. The dwell time of each event was a randomly generated number within the exponential distribution for that kinetic state. The following event was chosen based on the probability of going to each connected state. The amplitude of an open event was randomly chosen from a Gaussian distribution with a mean and standard deviation based on experimental amplitude histograms (constructed from idealized events). This accounted for an observed variation in mean amplitudes ($\pm 10\%$) that was not included in the model. The amplitude of each event was stored along with the dwell time. The list of events stopped when the sum of the dwell times reached the maximum time of the record designated by the operator. Next, the simulated data were sampled with the same protocol employed for the experimental data. Events were sampled at 25 kHz, and random Gaussian noise was added to the sampled data (± 0.25 pA, about the mean amplitude of the baseline, the noise typically observed at 5 kHz). These data were put through a Gaussian filter program (Colquhoun and Sigworth, 1995) with a 5-kHz cutoff frequency. To simulate the playback step, data were resampled at 5 kHz and filtered at 1 kHz. The resulting simulated data could be plotted as single channel traces (amplitude versus time). Events lists were compiled as described above, and subsequently analyzed just as those obtained from experimental data. Once the simulation of a connected state model produced parameters that came close to the experimental parameters, the rate constants in the connected state diagram were adjusted by small degrees, where necessary, to reproduce the parameters more closely. In all cases, the rates between states were adjusted to comply with the principle of microscopic reversibility. For this, the lifetimes of individual states were constrained, but the proportions of events that went to adjacent states were adjusted. It should be noted that a single exponential component may harbor several hidden states, so what we have called a single state could be a group of states with an average lifetime represented by a single time constant.

results

Behavior of Locked Channels and Comparison to Channels Activated by Free cGMP

Fig. 1 shows the opening behavior of single CNG channels locked in each liganded state. When one ligand was bound, the channel opened with very low probability and mostly to a low conducting level. With two ligands, the channel opened to multiple conducting levels, and entered into a bursting behavior characterized by frequent openings separated by brief closures. Three ligands caused significant opening, and each conducting level exhibited transient and sustained life times (see also below). In the fully liganded channel, the probability of opening approached unity. Moreover, the most prominent opening was to the highest conducting level. Overall, the behavior of the channel locked into any particular liganded state was intricate, indicating an intrinsic flexibility of the protein.

The flexible nature of the protein was particularly clear in triply liganded channels, where the probability of opening was large enough to allow examination of the myriad states and behaviors. Fig. 2 A shows a longer record ($\sim$5 s out of 100 s total) of a triply liganded
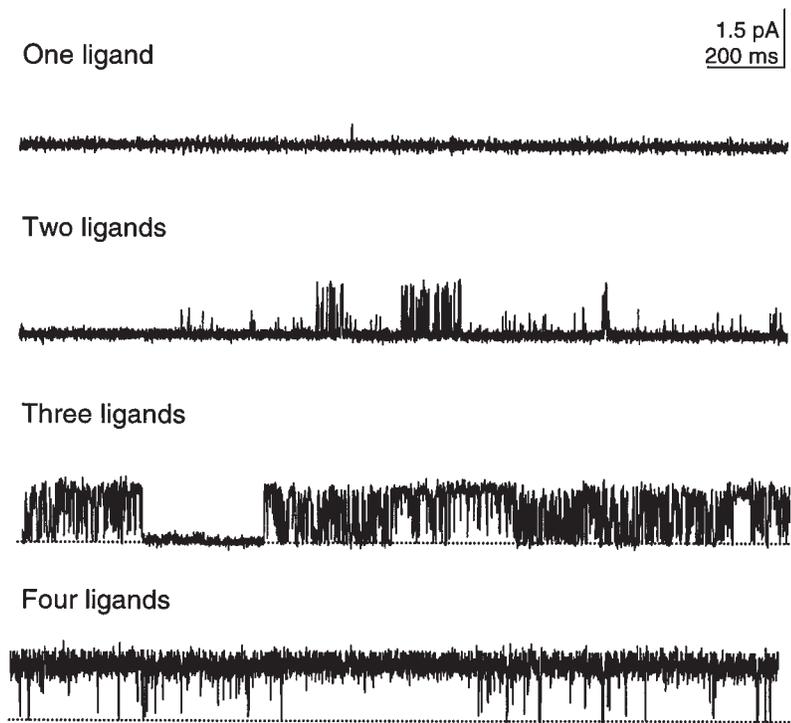
FIGURE 1. Behavior of locked channels portrays protein flexibility. Single rod CNG channels were activated by locking one, two, three, and four ligands into the cytoplasmic binding sites. Long sweeps of 2-s each illustrate the variety of behaviors the channel undergoes in the absence of binding and unbinding events. Most obvious are bursting behavior (two and three ligands), transient and sustained openings (three ligands), and very long-lived openings (four ligands). Openings to three conductance states are also apparent even on this long time scale (e.g., two ligands). Single channels were recorded at +50 mV. Data were from four different patches.
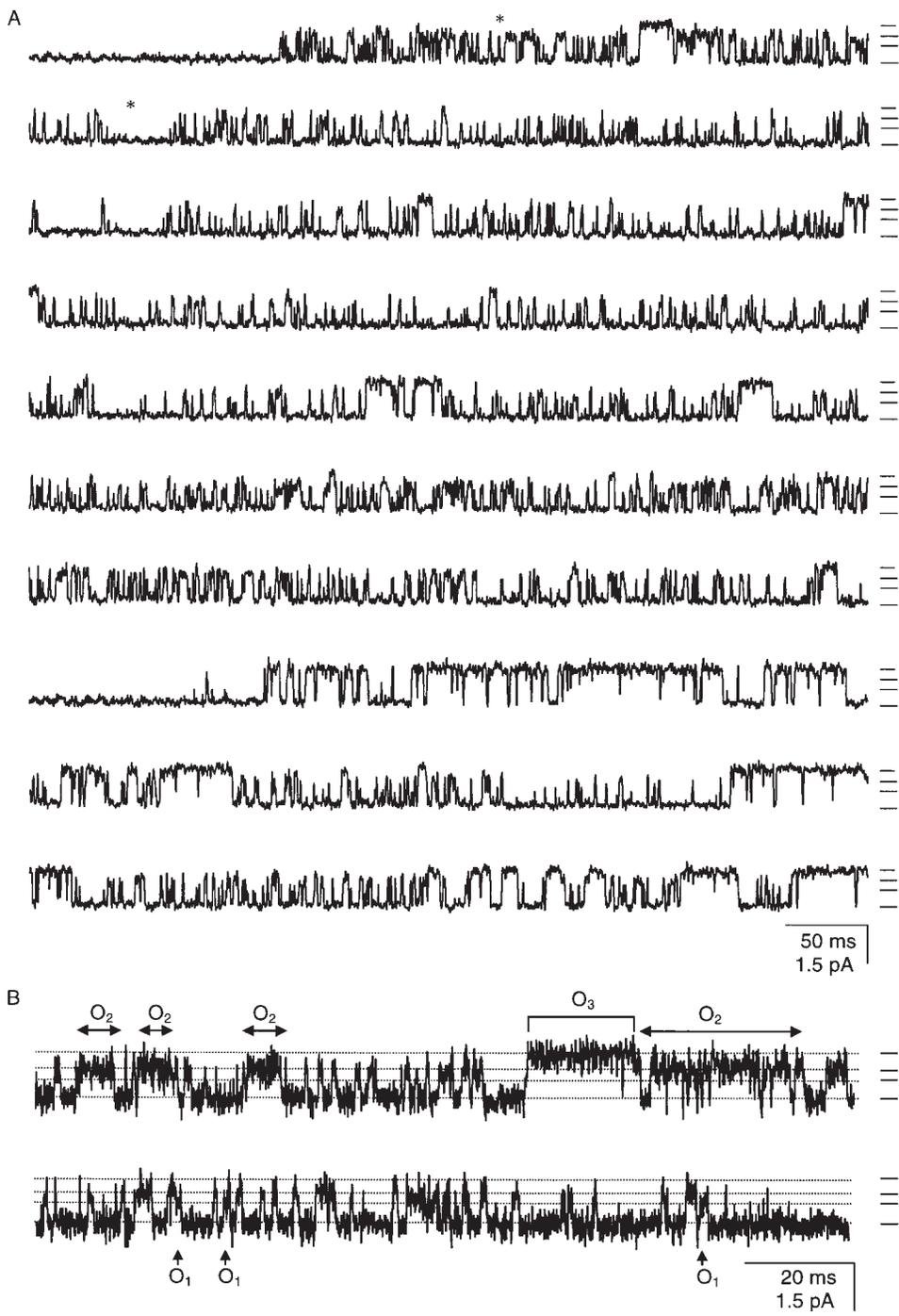
FIGURE 2. Subconductance states are most prominent in triply liganded channels. (A) The behavior of a single channel with three ligands covalently attached is shown (consecutive traces, 512-ms each). Horizontal lines at the right of each trace indicate the mean amplitudes of each conductance state (from bottom to top): 0 (closed), 0.6 (O1 state), 0.9 (O2 state), and 1.45 (O3 state) pA. Note that this channel opened mostly to the O2 conductance state, but O1 and O3 states are also easily distinguished. Record was filtered at 1 kHz. (B) The same data (section of A between the asterisks) filtered at 5 kHz is shown for better resolution of fast events. Horizontal lines indicating approximate mean current amplitudes for the three conducting levels were drawn by eye. Clearly, sustained openings to subconducting states (O1 and O2, as indicated) were more common than fast events that were cut off by filtering at 1 kHz.

channel on an expanded time scale. The small horizontal lines at the right of each trace indicate the mean current levels for the closed state (C), two subconducting states (O_1 and O_2), and fully open state (O_3). A fascinating and prominent feature was the tendency to open to subconducting states. In fact, the triply liganded channel preferred opening to these states over the fully open state. Many of the openings to subconducting states were quite stable, as shown in the stretch between the two asterisks. These states did not

arise from overfiltering of fast events as shown in the same stretch filtered at 5 kHz (Fig. 2 B) instead of 1 kHz (Fig. 2 A). Note in particular the long sojourns into the O_2 state. In the catfish olfactory CNG channel, rapid subconductance states have been shown to arise from protons binding in the pore (Root and MacKinnon, 1994). However, the entire record in Fig. 2 argues against subconductance states being the result of proton block in the rod channel. For example, if proton block were responsible for some of the briefer open-

ings to subconductance states as in row 2 of Fig. 2 A, then it would be difficult to explain the absence of proton block in row 8 and elsewhere during long openings. We cannot completely rule out the possibility that different conformational states could have different susceptibilities to proton block; however, this scenario would simply support our contention that locked channels are flexible and can assume a variety of conformational states. It should be recognized, however, that proton block of this channel has never been demonstrated at this pH (7.6) and membrane potential (+50 mV) (e.g., Tanaka, 1993; Picco et al., 1996), and that subconducting behavior was indistinguishable at pH 8.6 and +50 mV (Ruiz and Karpen, 1997). These latter conditions have been shown to eliminate proton block in the catfish olfactory CNG channel (Goulding et al., 1992).

There are several features apparent in locked channels that are usually assumed to arise from the binding and unbinding of free ligands. For comparison, the properties of single channels activated by free cGMP are illustrated in Fig. 3. At low ligand concentrations, the channel exhibited bursting behavior, openings to the same three current levels (Fig. 3, inset, and see Fig. 4 D), and both transient and long-lived openings; at saturating ligand concentrations (200 μM cGMP, Fig. 3), long, stable openings (*) occurred. Bursts are normally thought of as periods of repeated openings arising from highly liganded states, while the intervals between bursts are attributed to latency of binding. However,

Figs. 1 and 2 illustrate that bursting also occurred in locked channels, in the absence of binding and unbinding of free ligands. Subconductance states are thought on occasion to be an obligatory consequence of a multiply liganded channel losing one or more ligands (e.g., Ildefonse and Bennett, 1991; Rosenmund et al., 1998). However, in each liganded state, the locked channel freely moved between three conductance states without the loss or gain of ligands. Finally, both transient and sustained events were observed in locked channels. With three ligands attached (Fig. 1), the appearance of stable openings in the middle of a burst of rapid transitions is striking. Such different lifetimes are usually thought to reflect transient and stable binding events. However, the channel can exhibit these behaviors independent of ligand binding and unbinding.

There are two reasons to believe that these locked channel behaviors do not arise from tethered cGMP moieties momentarily "falling out" of the binding site. First, the length of the linker chain in APT-cGMP is very short (<10 Å) so that if the cGMP moiety unbinds, its effective concentration is expected to be on the order of hundreds of millimolar at that single cGMP binding site. Thus, unbinding events would be undetectable (<0.1 μs) within our time resolution. Second, if the effective concentration (which would dictate the tendency to rebind after unbinding) were much less than expected, we should be able to measure an increase in opening probability when free ligand is added to locked channels that are fully liganded. However, ad-

10 μM cGMP

20 μM cGMP

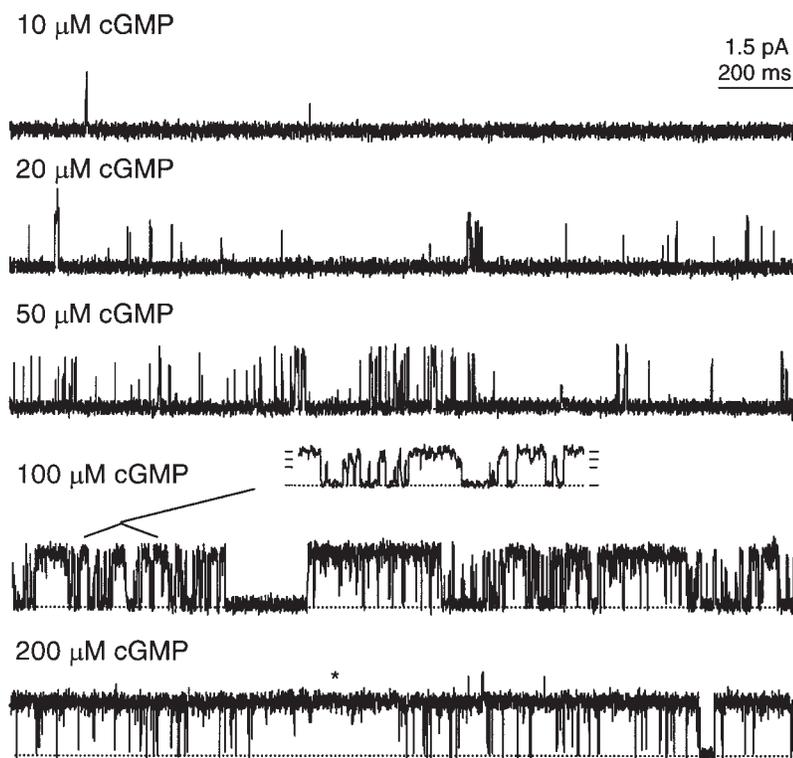50 μM cGMP

100 μM cGMP

200 μM cGMP

FIGURE 3. A single channel activated by free cGMP exhibits features similar to those observed in locked channels. Recording conditions were the same as above, except no ligands were locked on this channel. Instead, cGMP was added to the control solution. Bursting is apparent at low cGMP concentrations. Both transient and long-lived openings occurred. Very long openings (*) occurred in saturating cGMP concentrations. The channel opened to three conductance states: the inset shows 200 ms at 100 μM cGMP; horizontal ticks at right indicate closed and three open states: 0 (closed), 0.7 (O1 state), 1.0 (O2 state), 1.3 (O3 state) pA.

dition of 2–1,000 µM cGMP never increased the open probability of fully liganded channels. It is clear that locked channels exhibit many of the same properties as channels activated by free ligand. This indicates that intricate behaviors are intrinsic to the channel protein.

We now consider subconductance states in more quantitative detail. All partially liganded channels showed a preference for opening to subconductance states over the fully open state. This is demonstrated in the amplitude histograms in Fig. 4 A, which represent extended periods of channel behavior at each level of liganding. Channel opening with one ligand attached was similar to spontaneous channel opening, even though singly liganded channels required fewer ligands
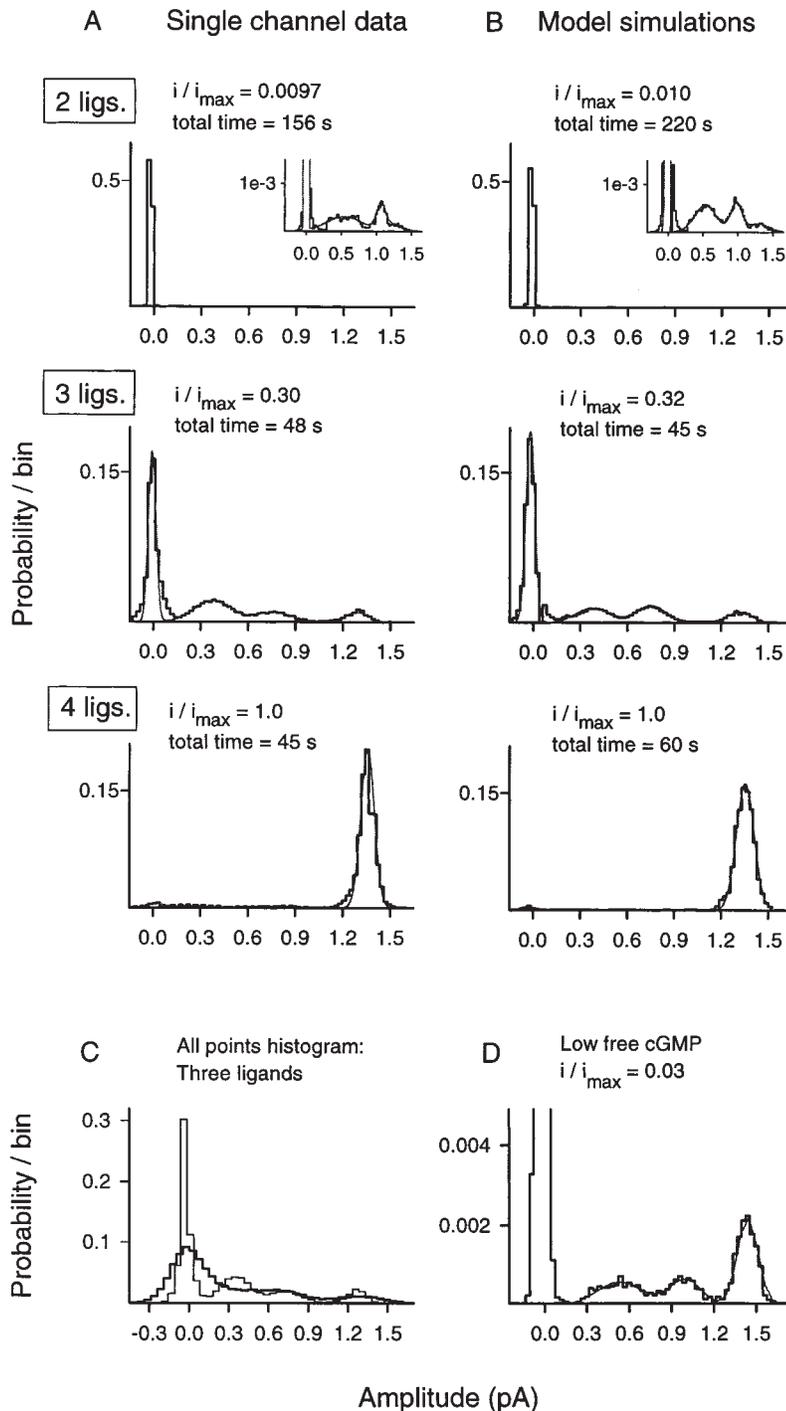

FIGURE 4. Amplitude histograms show locked channels open to multiple conductance states. (A) Amplitudes are from lists of events compiled with multiple thresholds (see MATERIALS AND METHODS). Probability density is plotted on the ordinate such that the total area of each histogram is equal to 1. The total time (after removing long closed times, see MATERIALS AND METHODS) of channel activity is noted above each plot. At each level of liganding shown, four Gaussians were required to fit amplitude distributions. Partially liganded channels (top and middle) favored opening to subconductance states over opening to the fully open state. The fully liganded channel (bottom) opened mostly to the fully open state. Areas under the peaks (closed, O1, O2, O3) are: two ligands, 0.988, 0.007, 0.003, 0.002; three ligands, 0.492, 0.285, 0.140, 0.083; four ligands, 0.035, 0.029, 0.024, 0.908. The total number of events were: two ligands, 15,057 events; three ligands, 39,427 events; four ligands, 13,270 events. I/I_{max} values are calculated as the mean current from a locked channel divided by the maximum current measured in the same channel at a saturating concentration of cGMP. Variations in I/I_{max} ranged up to sixfold between partially liganded channels: doubly liganded ($n = 3$), 0.0097, 0.0032, 0.0018; triply liganded ($n = 4$), 0.33, 0.25, 0.058, 0.052. The two lower values for triply liganded channels were from patches that had persisted for several hours and were exhibiting numerous long closed periods; therefore, we considered the two higher values to be more reliable. (B) Amplitude histograms from simulated traces. Areas under the peaks (closed, O1, O2, O3) are: two ligands, 0.983, 0.009, 0.005, 0.003; three ligands, 0.570, 0.168, 0.171, 0.091; four ligands, 0.021, 0.008, 0.009, 0.961. The total number of events were: two ligands, 16,833 events; three ligands, 47,251 events; four ligands, 10,572 events. (C) All points histogram gives the same result as fitted events histograms. An all points histogram (dark line) was compiled for the same data as shown above (A) for the triply liganded channel (light line). Although the peaks are broader in the all points histogram, a similar fit with four Gaussians was required. Mean amplitudes and areas under the peaks (closed, O1, O2, O3) are: 0 pA, 0.752; 0.2 pA, 0.113; 0.7 pA, 0.091; 1.2 pA, 0.043. (D) Average amplitude histogram of five single channel patches activated by low concentrations of cGMP. At low levels of activation (average $I/I_{max} = 0.03$ [range 0.01 to 0.05], $n = 5$), subconductance states contribute significantly to the total current. Areas under the curves are: 0.008 (O1), 0.006 (O2), and 0.013 (O3). The total number of events was 8,104.

to activate fully (data not shown; see Ruiz and Karpen, 1997). These openings, however, were very infrequent and did not allow for a detailed analysis. In doubly, triply, and even fully liganded channels, it is clear that the channel opened to multiple conductance states. A sum of four Gaussian functions, including one for the closed state, was required to fit the histograms with two, three, and four ligands attached (Fig. 4 A). All-points amplitude histograms, although naturally broader than histograms of idealized events (see MATERIALS AND METHODS), fully support the existence and prominence of subconductance states. Fig. 4 C shows a comparison of these two types of histograms for the same triply liganded channel record. Interestingly, different channels that had equal numbers of ligands attached (not shown) sometimes showed a preference for one subconductance state over the other (O1 or O2). However, partially liganded channels always had a higher probability of opening to subconductance states than opening to the fully conducting state. The overall degree of opening (I/I_{max}) in partially liganded channels also varied (see Fig. 4, legend). When four ligands were attached (Fig. 4 A), the channel favored opening to the fully conducting state (O3) at the expense of the subconducting states. Thus, opening to any given conducting state is dependent on how many ligands are bound. This is summarized in Fig. 5 A. In locked channels, both subconductance states peaked with three ligands attached. An important control for these experiments is the response of untethered channels to free ligand (Fig. 5 B). The individual dose–response relations revealed that the probabilities of observing both subconducting states peaked at the same concentration of cGMP. This is predicted from the results in Fig. 5 A. It should be noted that the probability of observing a subconductance state of the native rod channel also peaks at a subsaturating concentration of cGMP (Ildefonse and Bennett, 1991; Taylor and Baylor, 1995). Overall, the findings in Figs. 1–5 strongly support the notion that subconducting states are fundamental intermediate steps in the process of gating.

Probability of Opening of Locked Channels Explains the cGMP Dose–Response Relation

As a further test of whether data acquired from locked channels reflect the channel's natural response to cGMP, we determined whether the open probabilities predict the single channel dose–response relation. It is important to use a single channel dose–response relation for this analysis because the typically low Hill coefficient (~2.0) observed in macropatches does not reflect the consistently higher Hill coefficient (~3.0) observed in single channel patches (Ruiz and Karpen, 1997; Ruiz et al., 1999). A dose–response relation can be generated from locked channel data with the use
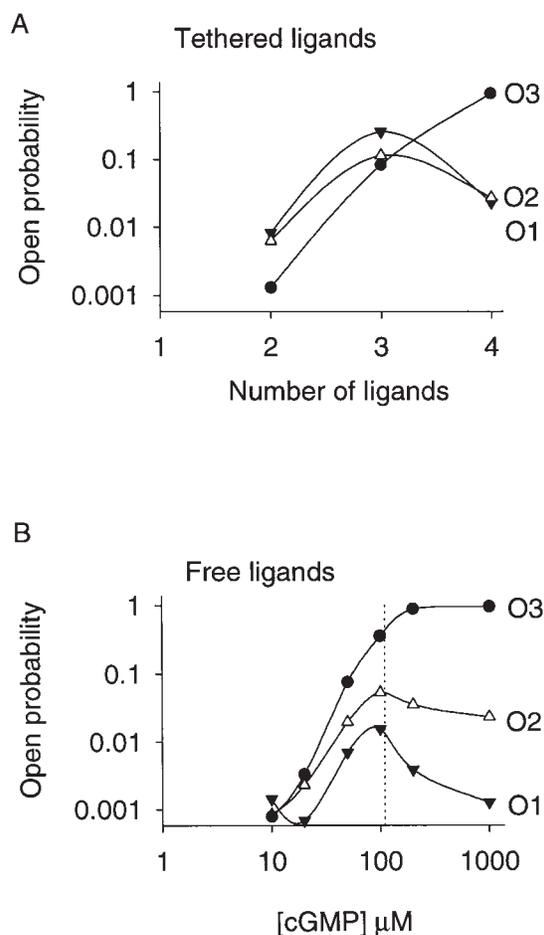

FIGURE 5. Occupancies of subconductance states exhibit a different ligand dependence than that of the fully open state. (A) Probabilities of opening to individual conducting states O1 (▼), O2 (△), and O3 (●) are shown for each liganded state. The probabilities of occupying both subconducting states (O1 and O2) peaked with three ligands bound. In contrast, the occupancy of the fully open state (O3) peaked with all four ligands bound. (B) The probability of opening to all three conductance states in a single channel activated by free cGMP shows the same trend. Again, the occupancies of both subconducting states peaked at the same subsaturating concentration of cGMP (dotted line indicates the $K_{1/2}$ value for this channel). The different proportions of openings to the O1 state observed in channels with four tethered ligands (A) and channels saturated with free cGMP (B) reflect variations among patches and are not correlated to covalent attachment of ligand. Similar results were obtained with three other channels.

of a minimum model (Fig. 6 A) that simulates the opening of locked channels as well as the binding of cGMP. We assumed initially that cGMP binds independently to the four identical subunits when the channel is in the closed state, and each liganded closed state opens to the degree predicted from the locked channel data. To simplify this analysis, the multiple open states we observed were contracted into a single open conformation. This is reasonable, because for a dose–response relation it is only necessary to know the overall
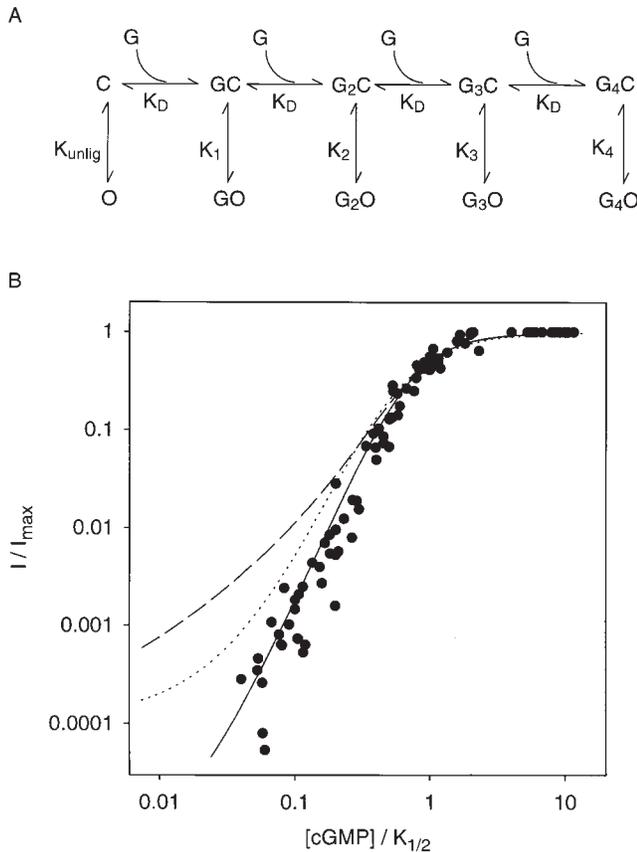
A

B

FIGURE 6. Data from locked channels are consistent with the single channel cGMP dose–response relation. (A) Minimum model used to simulate a dose–response relation from locked channel data. Cyclic GMP (represented as G) binds to each of four sites on the closed channel (C) with microscopic dissociation constant K_d. In each liganded state, the overall opening of the channel (to state O) is described by a single equilibrium constant: K_{unlig} when no ligands are bound, and K_1, K_2, K_3, and K_4 with the indicated number of ligands bound. First the I/I_{max} values describing the opening of channels locked in each liganded state (see text and Ruiz and Karpen, 1997) were converted into apparent open probabilities by multiplying by 0.95, the probability that a fully liganded channel is open. Then, the channel opening equilibrium constants were calculated as $P_o/(1 - P_o)$: $K_{unlig} = 6.5 \times 10^{-6}$, $K_1 = 9.1 \times 10^{-6}$, $K_2 = 9.3 \times 10^{-3}$, $K_3 = 0.46$, and $K_4 = 19$. The open probabilities of Liu et al. (1998) at each level of liganding, given in the text, were similarly converted to the following channel opening equilibrium constants: $K_{unlig} = 1.2 \times 10^{-4}$, $K_1 = 0.017$, $K_2 = 0.19$, $K_3 = 0.47$, and $K_4 = 19$. The only adjustable parameter, K_d, was assumed to be 100 μM. The open probability in the presence of different concentrations of free cGMP is predicted to be: $P_o = ([G]^4 K_4 + 4[G]^3 K_d K_3 + 6[G]^2 K_d^2 K_2 + 4[G] K_d^3 K_1 + K_d^4 K_{unlig})/\{[G]^4(1 + K_4) + 4[G]^3 K_d(1 + K_3) + 6[G]^2 K_d^2(1 + K_2) + 4[G] K_d^3(1 + K_1) + K_d^4 (1 + K_{unlig})\}$. The fraction of maximal current through a single channel at different concentrations of cGMP is given by $I/I_{max} = P_o(1 + K_4)/K_4$. This equation was used to simulate single channel dose–response relations. (B) Comparison of experimental and simulated single channel dose–response relations. ● shows data from 16 single channel patches. cGMP concentrations are expressed relative to each channel's $K_{1/2}$, the concentration that gave a half-maximal current (83–248 μM). This aligns the dose–response relations and allows the slopes to be compared. Simulated single channel relations were generated as described in A over a

881   Ruiz and Karpen

equilibrium between open and closed states. The degree of opening in locked channels can be expressed as the ratio of the mean current to the maximal current at saturation (I/I_{max}). These values were as follows: singly liganded, 9.6×10^{-6}; doubly liganded, 0.0097; triply liganded, 0.33; and fully liganded, 1.00. For this application, these values were converted to open probabilities and equilibrium constants as described in Fig. 6 A, legend.

Fig. 6 B shows dose–response relations from 16 single channel patches. I/I_{max} is the fractional current activated by cGMP. Because $K_{1/2}$ varied significantly between individual single channel patches, the cGMP concentrations were expressed relative to each channel's $K_{1/2}$. This simply aligned the dose–response relations along the x axis. The overall dose–response relation was fit with a Hill coefficient of 2.9, and the Hill coefficients for each single channel were also very high, ranging from 2.5 to 3.9. The solid curve shows a simulation from the model, which could be described by a Hill coefficient of ~ 2.8. As mentioned above, the opening of partially liganded channels exhibited some variability from patch to patch. For this simulation, the highest values were used because we felt these were the most reliable (see Fig. 4, legend). However, the lowest values (given in the legend) produced simulations that could be described by a Hill coefficient of ~ 3.1, which falls within the observed range of single channel Hill coefficients. The only free parameter in the model is the ligand dissociation constant, and the value of the Hill coefficient was virtually insensitive to changes in K_d. The reproduction of the dose–response curve is consistent with the idea that locked channels open normally, and is further evidence that the assignment of the numbers of tethered ligands in those channels is correct.

Liu et al. (1998) reported the following open probabilities for the different liganded states of mutated channels (see INTRODUCTION), which they regard as behaving like wild-type channels: singly liganded, 0.017; doubly liganded, 0.16; triply liganded, 0.32; and fully liganded, 0.95. Before this, the same group (Tibbs

wide range of cGMP concentrations. To compare with experimental data, the cGMP concentrations in the simulated relations were also expressed relative to the $K_{1/2}$ value for that simulation. The Hill equation: $I/I_{max} = [G]^n/([G]^n + K_{1/2}^n)$, where n is the Hill coefficient, was fit to the experimental data and to simulated relations that did not exhibit pronounced curvature. The solid curve shows a simulation based on our locked channel data, the dashed curve is a simulation based on the data of Liu et al. (1998), and the dotted curve is a simulation based on the coupled dimer model of channel activation proposed by Liu et al. (1998). For the latter simulation, we used the values of the parameters given in that study, with the exception of K_R, which was not given and is assumed here to be 4 μM. This yielded a $K_{1/2}$ value very similar to that obtained in the other simulations.

et al., 1997) reported spontaneous open probabilities in unliganded channels of 1.25×10^{-4}, which contrasts with an I/I_{max} value of 6.8×10^{-6} in our experiments (Ruiz and Karpen, 1997). The numbers from the former group suggest more opening of unliganded, singly, and doubly liganded channels. When we applied the same minimum model to test their open probabilities, the dashed curve in Fig. 6 B was obtained, which exhibits pronounced curvature and clearly cannot explain the wild-type single channel dose–response relations. Again, the simulation was insensitive to the value assumed for K_d. We also tested the effects of adding different degrees of binding cooperativity to closed states in the mechanism in Fig. 6 A, using K_d values that decreased progressively with each bound ligand. (It should be noted that favorable opening already confers a significant degree of binding cooperativity to the open states.) Using the opening numbers of Liu et al. (1998), the upper portions of the experimental relation (which are most sensitive to binding cooperativity) could be fit, but these simulations still deviated markedly from the foot of the relation (low I/I_{max} values). In contrast, adding an equivalent amount of binding cooperativity using our open probabilities yielded a good fit to the upper part of the curve and a slightly steeper fit to the foot of the relation that was still well within the spread of the data. The foot of the relation primarily reflects the number of ligands that have to bind for substantial activation, and significant deviations indicate discrepancies in the opening of lower liganded states. Finally, we tested whether a coupled dimer model proposed by Liu et al. (1998) could fit the single channel relations. In this model, four subunits associate as two functional dimers. Each dimer undergoes a concerted transition, and the channel opens when both dimers are activated in this way. Simulated data from this model (using the parameters of Liu et al., 1998) produced the dotted curve shown in Fig. 6 B. Although this is slightly closer to the wild-type dose–response behavior, it is still too shallow, and also exhibits pronounced curvature at low values of I/I_{max}. This model incorporates a significant degree of closed-state binding cooperativity like that described above. It comes closer to the foot of the experimental dose–response relations in Fig. 6 B largely because it predicts lower open probabilities in unliganded and singly liganded channels than those observed in the experiments of Liu et al. (1998). Later, we discuss possible reasons why their approach may have yielded somewhat distorted numbers for channel opening at different levels of liganding. In summary, locked channels appear to reflect accurately the activity of normally liganded channels; thus, we are confident in the reliability of this approach for dissecting the allosteric mechanism of channel opening.

Evaluation of Simple Allosteric Models

Eigen (1968) pointed out that the KNF sequential model (diagonal box) and the MWC concerted model (two vertical boxes) are both limiting cases of a more general allosteric model shown in Fig. 7. In this model, there are four subunits in a protein, each capable of undergoing a single conformational change (from □ to ○). The bound ligand is represented by G. In the KNF sequential model, ligand binding is required for conformational changes to occur; thus, for a tetrameric channel, different open states would arise with different numbers of ligands bound. Early studies of single retinal CNG channels seemed to support the sequential model, because subconducting states were observed at low cGMP concentrations and exhibited a dose dependence that suggested that they reflect intermediate steps in activation (Haynes et al., 1986; Zimmerman and Baylor, 1986; Hanke et al., 1988; Ildefonse and Bennett, 1991; Taylor and Baylor, 1995; see also Fig. 5 B). However, the sequential model is inadequate to describe the multiple open states observed at every level of liganding in locked channels (Ruiz and Karpen, 1997; and Fig. 4).
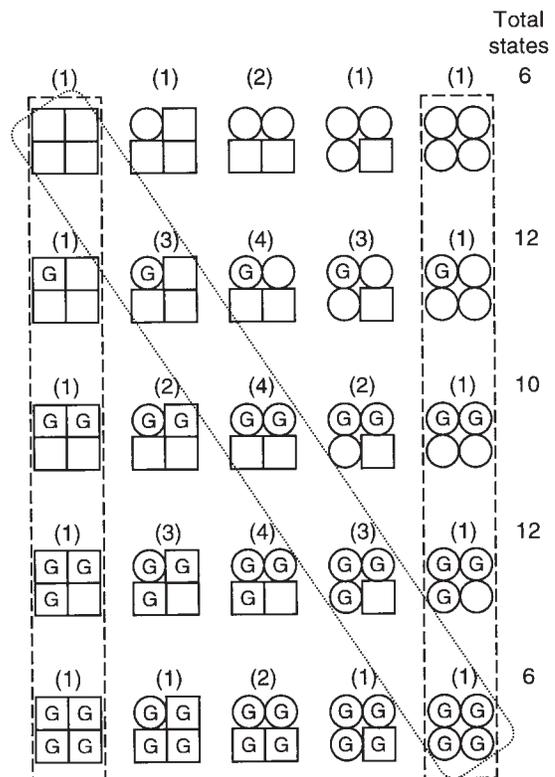

FIGURE 7. The general allosteric model in which each subunit can undergo a single conformational change. A complete description is given in the text. The sequential (KNF) model is outlined in a diagonal box, and the concerted (MWC) model is enclosed in two vertical boxes. The total number of distinct states for each row are listed at the right.

The MWC concerted model is a simple and appealing scheme that has been used to describe steady state, macroscopic current data for CNG channels. In this model, a channel protein assumes only two conformations, closed and open. The interconversion involves a synchronous change in all four subunits. Ligand binding increases the open probability by stabilizing the open conformation. Spontaneous channel openings in the absence of ligand have been reported for CNG channels (Picones and Korenbrot, 1995; Ruiz and Karpen, 1997; Tibbs et al., 1997). This finding is consistent with a concerted mechanism of opening; however, spontaneous openings are also predicted by the general allosteric model (see below). The very existence of subconductance states described above indicates that a two-state model is insufficient. Furthermore, at the level of resolution afforded by locked channels, it is clear that subconductance states were the most prominent open states in four of the five liganded conditions (zero to three ligands attached; Fig. 4). On occasion, the simple concerted model has been expanded to include two or three conformational transitions. An important prediction of any strictly concerted mechanism is that the channel opening equilibrium constant should increase by a constant factor with each ligand that binds. However, such models cannot describe our data because the overall equilibrium constants for each open (conductance) state did not change by a constant factor for each ligand that bound (Table I). The equilibrium constants (K_o) were calculated as the ratio P_o/P_c, where P_o is the probability of observing a particular open state, and P_c is the probability of observing the closed state. It is striking that for the two subconductance states the equilibrium constants not only did not change by a constant factor with each ligand (shown by the ratios of K_o between liganded states), but these factors actually varied by more than two orders of magnitude. The data for the fully conducting state are less complete since we rarely observed (and in some patches did not observe) this state with zero ligands or one ligand attached. However, kinetic data presented below argue strongly against concerted models even when the channel's opening behavior is simplified to consider only the fully conducting state.

In contrast, the general allosteric model in Fig. 7 captures some of the complex behavior that we have observed in single channels. For example, multiple channel conformations are allowed with a fixed number of ligands bound. In each row, the channel undergoes the same conformational changes regardless of the number of ligands bound. Thus, spontaneous opening of the unliganded channel is easily accommodated. The effect of ligand binding is to enhance the probability that those conformational changes occur. The actual scheme is more complex than the diagram shown, because a channel with a ligand bound to a subunit in a square conformation is different than a channel with a ligand bound to a subunit in a circle conformation. The total number of distinct states depends on assumptions about symmetry (recently reviewed in Cox et al., 1997). For the assumption of fourfold rotational symmetry, 55 distinct channel states are expected. This is a reasonable assumption for a channel with a single pore comprised of four identical subunits. With this assumption, adjacent subunits perform differently than diagonally opposed subunits. That is, if conformational changes occur in adjacent subunits, the channel behaves differently than if they occur in opposing subunits. Similar considerations apply to ligand binding to adjacent or opposed subunits. However, when ligands are locked into binding sites, only one binding configuration can be considered. This affects only the doubly liganded states (here, adjacent binding is assumed) and reduces the original 55 states to 46 total states (or 45 total states if two ligands bind to diagonally opposed subunits). Each state shown in the diagram represents the number of subunits that have undergone a conformational change ($\square$ to $\bigcirc$) and the number of ligands bound (G). The number of distinct states is indicated in parentheses above each representative state. For example, consider the case with three ligands bound, and three of the subunits have undergone conformational changes to a circle (row 4, column 4). There are three nonequivalent configurations possible. First, all three

t a b l e i

Overall Channel Opening Equilibrium Constants: Evaluation of Concerted Models

	One ligand			Two ligands			Three ligands			Four ligands		
	P	K_o	$\dfrac{K_o(1\text{lig})}{K_o(0\text{lig})}$	P	K_o	$\dfrac{K_o(2\text{lig})}{K_o(1\text{lig})}$	P	K_o	$\dfrac{K_o(3\text{lig})}{K_o(2\text{lig})}$	P	K_o	$\dfrac{K_o(4\text{lig})}{K_o(3\text{lig})}$
Closed	0.9994	—	—	0.9846	—	—	0.5487	—	—	0.0310	—	—
O1	6.2×10^{-5}	6.2×10^{-5}	~ 1	0.0080	0.0082	130	0.2549	0.465	56	0.0226	0.730	1.6
O2	$<10^{-5}$	$<10^{-5}$	~ 1	0.0062	0.0064	>640	0.1142	0.208	32	0.0268	0.865	4.2
O3	$<10^{-5}$	$<10^{-5}$	—	0.0012	0.0013	>130	0.0822	0.150	120	0.9196	29.7	200

P, probability of occupying a given state; K_o, P_o/P_c (opening equilibrium constant); $K_o([x + 1]\text{lig})/K_o(x\text{lig})$, the factor by which the opening equilibrium changes in going from a lower liganded state to the next higher liganded state.

subunits with ligand bound could be in the circle conformation, as shown. Alternatively, the unoccupied subunit could be a circle, and one of the three bound subunits a square. For the latter case, there are two possibilities. One is when the two bound circles are adjacent to each other, and the other is when the two bound circles are opposed to each other.

At each step of liganding, conformational changes that occur in one, two, three, or all four subunits are predicted to give rise to identifiable closed and open states. In evaluating the general allosteric model, locked channels allow us to examine channel opening behavior in each row, because the number of ligands attached is constant. We begin by examining channel behavior in the absence of ligand. The closed times for unliganded channels were fit with only one time constant ($\tau_c \sim 15$ s, not shown). Interestingly, spontaneous openings exhibited multiple conductance states. Although the most favorable was the lowest conductance state, the other two open states were occasionally observed, indicating that all three conductance states are an intrinsic property of the protein. The observation of multiple states is consistent with the general allosteric model; in fact, the model predicts more conformational states (6) than we observed (4). This may be due to the low probability of opening ($P_o \sim 10^{-5}$). Channel behavior with one ligand bound (Fig. 1) was not significantly different than the behavior observed in unliganded channels. Again, the low number of events may not allow for a meaningful test of the model.

For doubly, triply, and fully liganded channels, all states were sufficiently populated. Dwell-time histograms for closed states and each conductance state (O1, O2, O3) were constructed and plotted in Fig. 8 as the square root of the number of observations versus the $\log_{10}$ of the dwell intervals (Sigworth and Sine, 1987). This method allows a wide range of dwell times to be displayed. An additional advantage is that each exponential peaks at the value of its time constant. Interestingly, in the doubly liganded channel, the closed time distribution was fit with five exponentials. This indicates that the channel can assume at least five distinct closed state conformations. Triply and fully liganded channel closed time distributions required only three exponentials for a reasonable fit. Although we have already identified three open states based on different conductances, fits to individual open dwell-time distributions revealed multiple kinetic states. In some panels in Fig. 8 (e.g., C, F, and G), the need for two exponentials is not readily apparent. However, a single exponential would not accommodate all the long and short events; thus, some excess events would have to be omitted. First, we cannot justify omitting excess long-lived events because they contribute significantly to the overall open probability. Second, when a single exponential is constrained to accommodate the longest dwell times, excess brief events must be omitted. This results in simulated data with markedly fewer fast transitions, a prominent feature of single channel behavior (see Fig. 1). For the fully liganded channel, a third long-lived
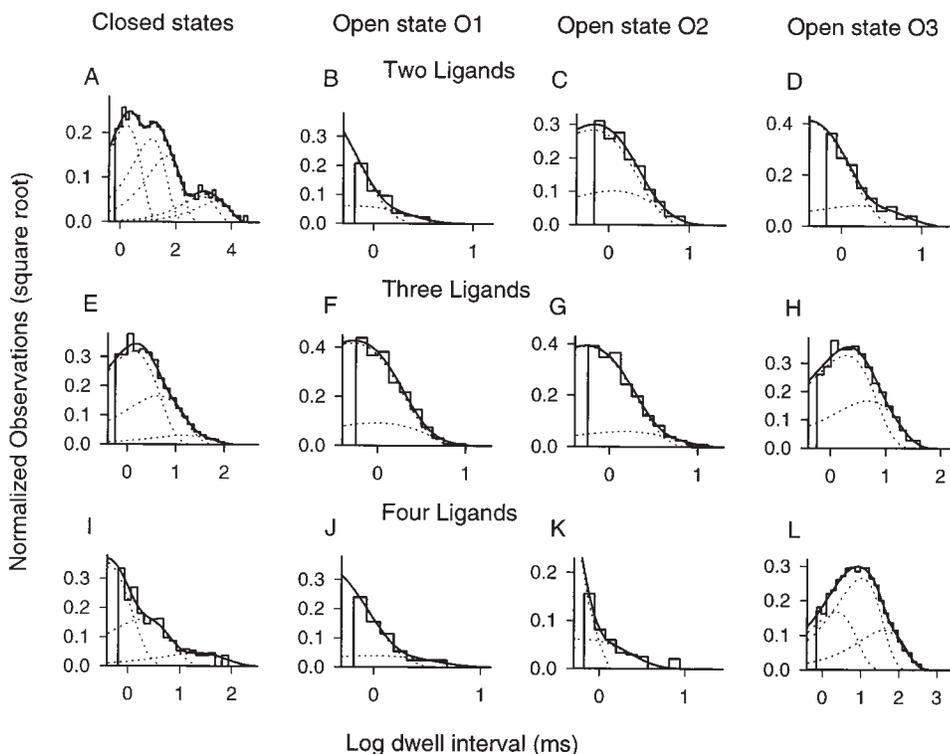
FIGURE 8. Multiple exponentials were required to fit dwell-time distributions for every conductance state. The square root of the number of observations was plotted against the $\log_{10}$ of dwell intervals so that widely disparate times could be displayed. Only dwell times ≥ 2 T_r were included in the fits (see MATERIALS AND METHODS). Maximum likelihood fits yielded exponentials that peak at the value of their time constants. Values for time constants, their fractional contributions, and the total number of events included in the fits for each distribution are given in Table II.

t a b l e   i i

Exponential Fits to Dwell-Time Distributions

	Single channel data						Simulations					
	Two ligands		Three ligands		Four ligands		Two ligands		Three ligands		Four ligands	
	τ	fraction	τ	fraction	τ	fraction	τ	fraction	τ	fraction	τ	fraction
	ms		*ms*		*ms*		*ms*		*ms*		*ms*	
C_{LLL}	2415	0.020	—	—	—	—	nd	nd	—	—	—	—
C_{LL}	705	0.030	—	—	—	—	698	0.027	—	—	—	—
C_L	40	0.200	15.4	0.010	11.5	0.014	49	0.120	10.0	0.012	14.8	0.001
C_M	11.5	0.320	4.30	0.220	1.60	0.170	12.07	0.400	3.80	0.227	1.29	0.104
C_S	1.45	0.430	1.30	0.770	0.28	0.816	1.56	0.453	1.20	0.761	0.243	0.895
$O1_S$	0.18	0.986	0.52	0.956	0.21	0.956	0.192	0.992	0.37	0.988	0.151	0.969
$O1_L$	0.67	0.014	1.00	0.044	0.69	0.044	0.994	0.008	0.97	0.012	0.541	0.031
$O2_S$	0.53	0.885	0.53	0.976	0.11	0.993	0.303	0.975	0.54	0.969	0.120	0.992
$O2_L$	1.00	0.115	1.50	0.024	0.635	0.007	1.284	0.025	1.10	0.031	0.567	0.008
$O3_S$	0.31	0.962	1.90	0.790	2.60	0.250	0.313	0.967	1.40	0.689	2.67	0.356
$O3_L$	1.45	0.038	4.90	0.210	9.10	0.630	1.525	0.033	4.90	0.311	12.5	0.507
$O3_{LL}$	—	—	—	—	34.0	0.120	—	—	—	—	46	0.137

nd, not done for simulations; fraction, fractional contribution to overall fit for that conductance level; total numbers of events included in the fits for each distribution (closed, O1, O2, O3) were, for real data: 4161, 1034, 1646, 414 (two ligands), 10374, 10810, 5630, 1548 (three ligands), and 551, 466, 206, 3748 (four ligands); simulated data: 6203, 695, 900, 340 (two ligands), 14175, 3988, 5669, 1393 (three ligands), and 836, 106, 165, 3894 (four ligands).

open state was observed that was not apparent in partially liganded channels (Fig. 8 L). As an important control, the dwell times for O3 were fit with the same three exponentials in channels activated by saturating free cGMP, though the proportion of the longest-lived state ($O3_{LL}$) was slightly lower than that observed in locked channels (data not shown; see also Nizzari et al., 1993). Table II lists the time constants and their fractional contributions for all liganded states that were fully analyzed.

Since the fully liganded channel record was filtered at 1 kHz, we were concerned that very short events in between O3 open times could have been missed, thus giving rise to artifactually long open events. To check whether the longest component was real, the same record filtered at 5 kHz was analyzed. The open channel noise was high (root mean square = 0.28 pA), and it was difficult to distinguish noise spikes from rapid events (false event detection rate $\sim$450 s^{-1}). Thus, we chose to compile indiscriminately all events that crossed a threshold set midway between the bottom of the open channel noise and the O2 level. Afterwards, a resolution of 80 μs was imposed (Colquhoun and Sigworth, 1995) (the filter rise time is 70 μs at 5 kHz, as opposed to 340 μs at 1 kHz). The maximum likelihood fits (not shown) to all O3 events detected in this analysis still required three exponentials with the following time constants and proportions: 1.6 ms and 0.113; 7.8 ms and 0.867; and 23 ms and 0.02 (7,128 total events). The proportion of the longest component was lower; however, this was expected with such a high false detection rate and a threshold set very close to the noise level. The important result was that three components

were still measured. Thus, the filtering at 1 kHz did not produce a third component that was not real. It should be noted that when records like this are corrected for missed events, the number of components usually does not change, although the time constants and proportions may be altered (Colquhoun and Sigworth, 1995).

Overall, the kinetic analysis indicates that there were 11 distinguishable states in doubly liganded channels, 9 in triply liganded channels, and 10 in fully liganded channels. The general allosteric model described above predicts 10 states in doubly liganded channels, 12 in triply liganded channels, but only 6 in fully liganded channels. (It should be noted that an alternative assumption of twofold symmetry still predicts only seven states in the fully liganded channel.) This model comes close to accounting for the number of states observed in our single channel data. However, the large number of states in the fully liganded channel points out that we need to expand on the general allosteric model by allowing for more than one conformational change per subunit. To evaluate fully the general allosteric model or any expanded version, it is necessary to determine how the various channel states are connected to each other and what the transition rates are.

Development of a Connected State Diagram

The first question is whether each conducting level can arise directly from a closed state, or whether closed states always open to a particular conducting level. A simple inspection of the raw records from doubly, triply, and fully liganded channels indicates that all conducting states can directly follow a closed state. The sec-

ond question is whether the different conducting states are connected to each other. Again, simple inspection indicates that the conductance states are connected to each other. Finally, given that there are multiple closed states and open states, we would like to know which individual states are directly connected to each other. We considered using maximum likelihood methods, but the large number of states and the presence of stable subconductance states made these methods impractical. Thus, we examined the connections between individual closed and open states by means of an adjacent

state analysis (Magleby and Song, 1992; Colquhoun and Hawkes, 1995; Rothberg et al., 1997). An assessment of bursting behavior was used to corroborate the adjacent state analysis. We then used simulations to test the models, which also provide a realistic correction for missed events. The APPENDIX describes how the adjacent state analysis, burst analysis, and model simulations led to the development of a connected state model.

We found that the single connected state model shown in Fig. 9 A, with rate constants given in Table III, could explain the kinetic data for doubly, triply, and
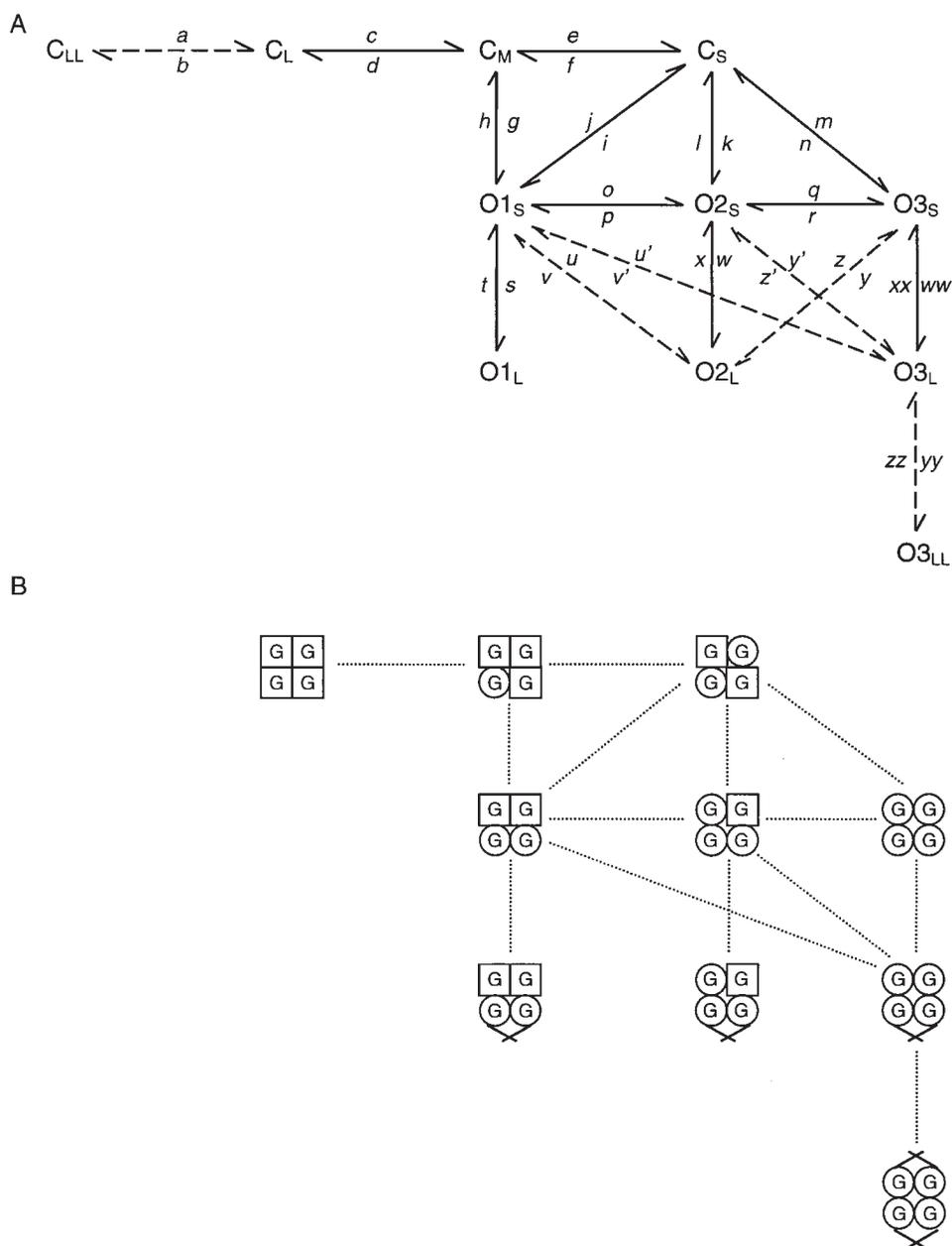

FIGURE 9. A similar connected state diagram can explain channel behavior in each liganded state. First, three conductance levels were always observed. Second, the shortest closed state always opened to all three conductance states. Third, the number of total states was similar at each liganding step. (A) Empirical connected state diagrams are superimposed for the three liganded states analyzed. The three short-lived open states ($O1_S$, $O2_S$, and $O3_S$) are connected to long-lived open states differently for the doubly liganded channel (u, v, y, z) than for the triply and fully liganded channels (u', v', y', z'). Dashed lines indicate transitions that are not observed at every level of liganding. For instance, the longest closed state (C_{LL}) and the longest open state ($O3_{LL}$) are observed only in the doubly and fully liganded states, respectively. Individual rate constants (a–zz) are given in Table III. (B) A plausible extension to the general allosteric model can account for the number of closed and open states in the empirical connected state diagram. Here, the last row (fully liganded channel) of the general allosteric model has been extended with four extra conformational states. These extra states arise from a putative change in the association of adjacent subunits that have bound cGMP and are in circle conformations. When two or three subunits are in circle conformations, one adjacent pair can alter their association, thereby giving rise to a long-lived sub-

conductance state ($O1_L$ or $O2_L$, respectively). When all four subunits are in circle conformations, one or both pairs can change their association, giving rise to $O3_L$ or $O3_{LL}$. However, entrance into these long-lived states is dependent on the favorability of occupying the short open states.

<div align="center">

t a b l e   i i i

Rate and Equilibrium Constants for the Connected State Model in Fig. 10

</div>

Rates	a	c	e	g	i	k	m	o	q	s	u	u′	w	y	y′	ww	yy
s^{-1}	b	d	f	h	j	l	n	p	r	t	v	v′	x	z	z′	xx	zz
Two ligands	2	25	7	78	410	295	16	282	394	99	50	—	54	96	—	157	—
	6	15	50	2620	1914	2189	583	442	1920	935	396	—	273	103	—	712	—
K_{eq}	0.3	1.7	0.1	0.03	0.2	0.1	0.06	0.6	0.2	0.1	0.1	—	0.2	0.9	—	0.2	—
Three ligands	—	38	78	112	702	106	7	759	95	9	—	41	4	—	33	34	—
	—	3	52	98	920	263	91	1415	502	690	—	145	586	—	63	12	—
K_{eq}	—	13	1.5	1.1	0.8	0.4	0.08	0.5	0.2	0.01	—	0.3	0.007	—	0.5	2.8	—
Four ligands	—	86	336	243	415	632	2308	229	868	238	—	3099	46	—	3420	119	13
	—	14	152	245	925	1523	231	254	36	1506	—	35	752	—	35	28	29
K_{eq}	—	6.1	2.2	1.0	0.4	0.4	10	0.9	24	0.2	—	88	0.06	—	98	4.2	0.4

In each column, forward rates are on the top line and backward rates are below. Rate constant designations between states (a–zz) are as shown in Fig. 10. K_{eq} are equilibrium constants (forward rate/backward rate) between states in each column.

fully liganded channels. The solid lines indicate connections that were used in all three liganded conditions, while the dashed lines indicate connections that were necessary to simulate data in only one or two of the liganded conditions. An additional closed state was observed in doubly liganded channels (C_{LL}) and an additional open state was observed in fully liganded channels ($O3_{LL}$). Furthermore, different connections between long-lived open states were used to simulate the behavior in doubly liganded versus triply and fully liganded channels. In triply and fully liganded channels, long-lived openings to the O3 states were interrupted by rapid transitions to and from the subconductance and closed states (see Fig. 1). This pattern was simulated most easily by connecting state $O3_L$ and the two short-lived conductance states ($O2_S$ and $O1_S$), instead of connecting the long-lived open states.

Comparisons between real and simulated single channel traces for the three liganded conditions are shown in Fig. 10. Amplitude histograms are compared in Fig. 4, A and B, dwell-time constants are compared in Table II, and the adjacent state analyses (see APPENDIX) are compared below in Fig. 11 and Table IV.

Clearly, the connected state diagram in Fig. 9 A reproduces most of the single channel characteristics. We do not propose that this connected state diagram is unique. For instance, equivalent states could have been missed by equating the number of exponentials with the number of distinct states. However, adding more states does not change the main conclusion that locked channels can assume a large number of stable kinetic states. Including a larger number of states would probably obviate the need for diagonal connections in Fig. 9 A. Also, it may have allowed us to capture some of the more complex single channel behavior. For example, the tendency for short- and long-lived events to occur in clusters is not fully reproduced. Also, the bursting properties were similar, but not as robust as observed in the data (see Table V). At this resolution, however, there is not enough information to include more states. The fact that the data at each liganded level is reproduced by similar diagrams lends credence to the notion that the channel assumes a similar set of conformational states. Thus, this feature of the general allosteric model shown in Fig. 7 is supported by the data, where each row could be represented with the con-

Locked Channels Simulations

1.5pA
50 ms

Two Ligands
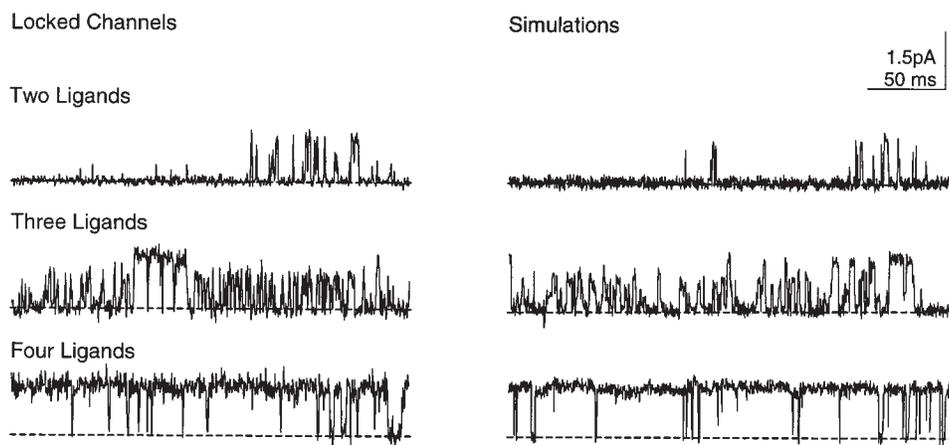
Three Ligands

Four Ligands

FIGURE 10. Simulated traces (right) reproduce most aspects of channel behavior observed in traces from locked channels (left). Bursting behavior is evident with two ligands bound, openings to subconductance states are predominant with three ligands bound, and long, stable openings prevail when four ligands are bound. In addition, both transient and sustained events are evident at all levels of liganding.

nected state diagram. However, a single conformational change as depicted in the general allosteric model is insufficient to account for all the states observed in the connected state model. A plausible extension of the general allosteric model is discussed below.

Although there are details of our model that remain uncertain, there are several salient features that emerge from this analysis. First, subconductance states are ligand dependent and are particularly prominent in triply liganded channels. Thus, any successful model will have to include subconductance states as critical intermediate steps in gating. Furthermore, models will have to include multiple kinetic states at all conducting levels. Another noteworthy feature is the tendency for bursting behavior to transpire without binding and unbinding of ligand. This bursting occurs at intermediate levels of liganding, when the channel is observed to leave absorbing closed states, and then shuttle between activated closed and open states. This suggests that in locked channels two or more ligands give rise to bursts by overcoming an energy barrier between the absorbing closed states and the activated states. Conversely, in fully liganded channels, open states are so favorable that returning to absorbing closed states is rarely observed. This behavior is described by the connected state model and a mechanism for bursting very much like this will have to be incorporated into any successful model. Another feature that is essential to any model is that in the fully liganded channel there is a direct, favorable path from an activated closed state to a stable, long-lived fully open state. That is, opening to the O3 state rarely occurs in a staircase fashion (through subconductance openings). Such a sequential mechanism appears to be operating in glutamate receptors (Rosenmund et al., 1998). However, in those channels, even when one conductance state predominates (proposed to arise from a particular liganded state), there are brief transitions to other states. These transitions might reflect a flexibility in those channels similar to that observed in the rod CNG channel.

discussion

Mechanistic Implications of Locked Channel Data

To determine the effects of ligand binding on conformational changes in allosteric proteins, investigators have generally been limited to adding different concentrations of free ligand. Even in single channel recording, in which there is an unprecedented resolution of conformational states, it is difficult with this limitation to assign any observed behavior to a particular liganded state. At any instant, it is virtually impossible to know how many ligands are bound. Taking advantage of a method we developed for covalently tethering

ligands to single CNG channels (Ruiz and Karpen, 1997; Brown et al., 1993), we have presented here a complete kinetic analysis of single rod CNG channels locked in each liganded state.

Remarkably, we have found that channels with a fixed number of ligands in place exhibit interconversions among 9 or 10 different states: 4 different conductance levels (including closed) and more than 1 kinetically distinguishable state at each of those conductance levels. Many of these states were stable on the millisecond time scale. The large number and complex behavior of states (Fig. 2) cannot be explained by simple phenomena such as proton block, which has been shown to cause two rapid subconductance states in catfish olfactory CNG channels (Goulding et al., 1992; Root and MacKinnon, 1994). The number of conducting states we observed at each liganded level is clearly inconsistent with either simple concerted (MWC) or sequential (KNF) allosteric models. An attempt to explain the behavior with a somewhat more complicated concerted model in which each conducting state arises from a separate concerted transition from the closed state also fails: when each conducting level is treated as a single state, the apparent channel opening equilibrium constant does not change by a constant factor with each ligand that binds (Table I). Most importantly, the observation of two to five kinetically distinguishable states at each conducting level violates both the letter and intent of strictly concerted models, which were proposed for their simplicity. However, with some limitations to our resolution of the precise rate constants for the different kinetic states, and lacking detailed structural information, we cannot rule out that there are some concerted transitions in the channel's activation pathway (see Varnum and Zagotta, 1996).

The fact that approximately the same number of states were observed in doubly, triply, and fully liganded channels suggests that the channel undergoes the same series of conformational changes. On this idea, different numbers of bound ligands would favor certain states over others. The success of the connected state model (Fig. 9) in simulating the intricate behavior in each liganded state lends strong support to this overall hypothesis. The number of distinct states that were observed at each level of liganding is most easily explained by assuming that there are activating conformational changes in each individual subunit. The general allosteric model (Eigen, 1968) shown in Fig. 7 postulates only a single conformational change per subunit, and yet it comes close to providing enough states. The only condition in which it obviously falls short is the fully liganded channel. The model postulates 6 states with an assumption of fourfold and 7 states for twofold rotational symmetry, while 10 states were observed. If this model is part of activation, the fact that it provides enough states at lower

levels of liganding could indicate either that there are additional conformations in fully liganded channels, or that these additional states exist in lower liganded channels but were not resolved. The latter could be due to limited kinetic resolution, to functionally equivalent states, or to some states not being sufficiently populated.

In comparing the general allosteric model with the connected state model (or, for that matter, with the behavior of any channel), it is not clear which states would be closed and which would be open. Given that there are four observed conductance states and five stages of activation in the model, the following assumptions seemed quite reasonable (Fig. 9 B): channels with zero and one activated subunits are closed; channels with two adjacent subunits activated give rise to an open state (O1), and channels with diagonally opposed subunits activated are still closed; channels with three and four activated subunits give rise to different open states (O2 and O3, respectively). This can account for all of the closed states and is enough (or more than enough) to account for the short-lived open states. However, multiple O3 states, which probably require all four subunits to be activated, are not easily explained. Furthermore, in the fully liganded channel, there are four states missing. We assume therefore that the four long-lived open states require additional conformational changes. The simplest way to expand the general allosteric model is by introducing a second conformational change per subunit. Such a scheme has been proposed for the activation of *Shaker* K^+ channels (Zagotta et al., 1994). In this scenario, the fully liganded state would be permitted 21 distinct conformations. While possible, this seems a bit of an overcompensation since the fully liganded state lacks only four open states. An alternative way to expand the model is by introducing a conformational change that requires a change in the association of two adjacent subunits that have undergone a square-to-circle conformational change (Fig. 9 B, crossed lines). In this speculative model, we can limit the number of total states by requiring that this association occurs only on adjacent subunits that have ligands bound. This predicts long-lived open states will occur only after at least two ligands are bound to the channel, in accordance with our observations. The longest-lived open state ($O3_{LL}$) would arise from the association of two pairs of subunits in unison, which is possible only in the fully liganded channel. Thus, the size of the conductance state (O1, O2, O3) could be determined by the number of subunits in the active conformation (circle conformations), and the lifetime (O_S, O_L, or O_{LL}) could be determined by whether or not adjacent subunits were interacting. Altogether, this adds three conformations each to the doubly and triply liganded states and four conformations to the fully liganded state.

Disparate regions of the channel protein have been reported to move during gating (see INTRODUCTION for references). This is not surprising given that binding of ligand in the COOH-terminal tail induces opening of the pore some distance away. These findings suggest that there is an intrinsic flexibility in each subunit, and lend support to our proposal that subunits undergo conformational changes in the absence or presence of ligand.

The connected state model allows us to examine whether these apparent subunit-based changes occur independently of each other or cooperatively. As closed states proceed from inactive to activated states (that lead to open states), it is clear that there is a progressive increase in rates, apparent in all liganded states (Table III). This contrasts with the expected decrease in rates (4α, 3α, 2α, α) that would be predicted by subunits behaving independently. This suggests that as each subunit undergoes a conformational change, it increases the probability that another subunit will do the same. Thus, these subunit-based conformational changes appear to be occurring cooperatively. Similarly, the rates from closed to open states do not appear to follow the pattern for independence. This makes it more difficult to predict the underlying structures for each state.

The speculative structural scheme in Fig. 9 B implies that some of the conformational changes can occur in more than one subunit simultaneously. These can be thought of as concerted transitions that occur alongside single subunit-based changes. Two types of concerted transitions are depicted in Fig. 9 B: diagonal lines indicating square-to-circle changes that occur simultaneously, and crossed lines indicating associations between adjacent subunits. Sometimes the concerted transitions would dominate (e.g., the transition between C_S and $O3_S$ in the fully liganded channel), and other times they would be relatively minor (e.g., the transition between C_S and $O1_S$ in the fully liganded channel). Regarding the proposed changes in association between pairs of subunits, there is evidence that interactions between adjacent subunits can stabilize the open state (Gordon and Zagotta, 1995b). These authors showed that Ni^{2+} potentiation, which stabilizes the open state, requires two histidine residues in adjacent subunits. In another study (Varnum and Zagotta, 1996), activation properties were different between homotetrameric channels that had two mutated subunits adjacent to each other compared with channels with the same two mutated subunits diagonally opposed to each other. Recently, Liu et al. (1998) proposed a mechanism that employs adjacent subunit interactions (coupled dimer model) as the only means of opening the channel. This model, however, was not based on any kinetic analysis. Here, we have shown that there are many more kinetic states than can be explained by

their two-step mechanism; however, we incorporate adjacent subunit interactions as a plausible means to extend the total number of conformational states of the general allosteric model. It is important to realize that, although the structural scheme depicted in Fig. 9 B can explain the number of observed states with only two types of conformational changes, there is no direct evidence for these particular structures.

Two Approaches for Studying the Contribution of Ligand Binding to Channel Gating

Liu et al. (1998) have recently taken issue with our assignment of the number of ligands attached to channel binding sites, based on discrete shifts (in $K_{1/2}$) in the cGMP dose–response relations (Ruiz and Karpen, 1997). They have suggested that spontaneous shifts in our dose–response relations led to mistaken liganding assignments; however, such spontaneous shifts have been ruled out in our experiments (see MATERIALS AND METHODS). An advantage of our method is that we are able to assess behavior in the same channel before and after tethering ligands. A large number of dose–response relations for single channels superimposed in the control condition (Fig. 6 B), making the subsequent shift caused by the attachment of one ligand unmistakable (Ruiz and Karpen, 1997). Most importantly, the P_o values obtained from locked channel data can reconstruct the dose–response relation obtained from unmodified single channels (Fig. 6). In contrast, Fig. 6 also demonstrates that it is difficult to reconstruct the single channel dose–response relation from wild-type channels using the data of Liu et al. (1998). This fit to unmutated, unmodified single channel data is crucial since both approaches introduce modifications to the normal ligand-bound channel.

We suggest that the data of Liu et al. (1998) are not consistent with the opening of wild-type channels either because extensive mutagenesis has altered channel gating or because their assignment of the number of active binding sites is incorrect. It remains a possibility that slightly different experimental conditions (e.g., high KCl on both sides of the membrane in their experiments) could have contributed to the observed differences. Nonetheless, the effect on gating that might be caused by substituting a foreign pore region into retinal channels (RO133 subunits containing a catfish olfactory CNG channel pore) has been studied only in homomultimeric channels and only at the macroscopic current level (Goulding et al., 1993). This is insufficient to determine whether single channel behaviors change. In this vein, subtle single amino acid mutations in the pore have been shown to alter gating (e.g., Bucossi et al., 1997). In addition, the mixing of replaced pore regions and multiple binding site mutations may

have unforeseen effects on gating. For example, in the study by Liu et al. (1998), a subunit with a double binding site mutation and a retinal pore expressed, while a subunit with the same double binding site mutation and an olfactory pore did not express.

Regarding the assignment of the number of active binding sites, Liu et al. (1998) may have missed singly liganded channels because they were limited to searching for robust channel activity with a well-defined conductance level. We have found that a singly liganded channel rarely opens, and when it did open it was usually to brief subconducting levels. Thus, discrimination between channels with a single active binding site and those with no active binding sites would be challenging. Their use of Ni^{2+} to improve the resolution of channel conductance may not be reliable because some channel constructs could not be potentiated, and it has not been shown which open states Ni^{2+} will stabilize. The variability of Ni^{2+} potentiation among channel constructs further suggests that the extensive mutagenesis affects gating.

The Potential Physiological Importance of Subconductance States

The low levels of channel activity (1–5%) that comprise the dark current of rod outer segments (Nakatani and Yau, 1988) suggest that under physiological conditions subconductance states are likely to play a role in phototransduction. Fig. 4 D shows an amplitude histogram averaged over five different channels in which free cGMP produced activation between 1 and 5% (3% average). Subconductance states were occupied roughly half the time [P_o(O1 + O2) = 0.014 and P_o(O3) = 0.013], and contributed about one third of the total current. Recently, Hackos and Korenbrot (1998) reported the intriguing result that the Ca^{2+}/Na^+ permeability ratio changes as a function of cGMP concentration in retinal rod outer segments, suggesting that subconductance states may play an important role in regulating internal Ca^{2+} concentrations.

Conclusions

Using a powerful approach that allows us to tether one ligand at a time to single CNG channels, we have presented a thorough kinetic analysis of channel gating at every level of liganding. The richness of channel behavior we observed indicates a complex mechanism of gating that has not been recognized before. Simple concerted and sequential mechanisms, as well as the simple coupled dimer model proposed recently, are easily ruled out. Instead, we propose that the same 10-state mechanism, including two subconducting levels and a fully conducting level, can explain gating in each liganded state. In structural terms, such a model can be
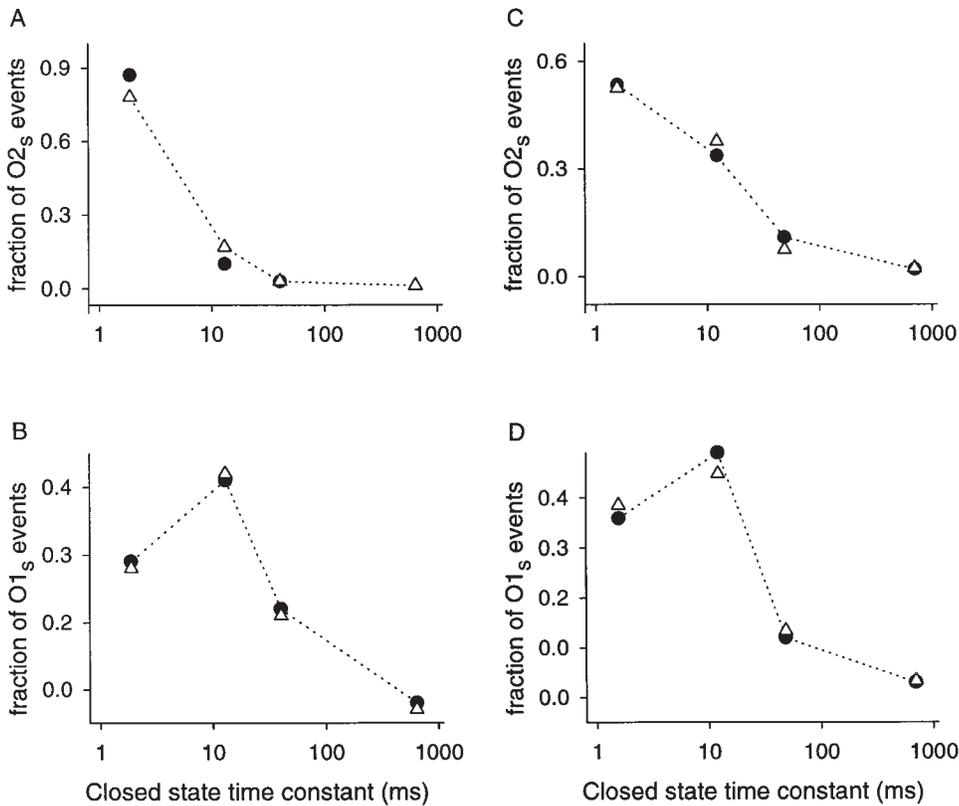
FIGURE 11. Adjacent state analysis indicates the most probable connections between states. (A) All closed events (≥ 2 T_r) adjacent to O2$_S$ were grouped as short and long events with ranges centered about the closed time constants (C$_{LL}$, C$_L$, C$_M$, and C$_S$). The proportions of O2$_S$ events that went to each closed state are plotted ($\bullet$). The same analysis was done with all closed events that opened to the O2$_S$ states, and the proportions are plotted ($\triangle$), for comparison. (B) Adjacent state analysis is shown for all O1$_S$ events that go to the closed states ($\bullet$). For comparison, the proportions of each closed state that opened to O1$_S$ are also plotted ($\triangle$). (C and D) Adjacent state analyses for simulated data show similar trends as those observed in real data (A and B).

accounted for by invoking more than one conformational change in each subunit.
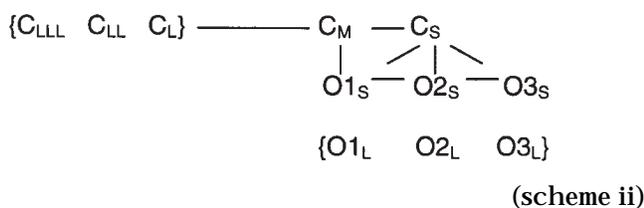
appendix

We present here adjacent state analysis, burst analysis, and model simulation procedures that led to a preliminary connected state model. The adjacent state analysis was simplified by grouping events into conductance states and then by studying connections between defined kinetic states. When this procedure (see MATERIALS AND METHODS) was applied to doubly liganded channels, strong evidence for two particular connections between open and closed states emerged. In Fig. 11 A ($\bullet$), the fraction of observations of the short-lived O2 state (i.e., number of O2$_S$ events followed by C$_S$/total number of O2$_S$ events that went to all closed states) is plotted as a function of the closed times that immediately followed (grouped by ranges centered at the values of the different closed time constants). It is clear that the highest proportion of O2$_S$ openings decayed to the shortest closed state (C$_S$), suggesting that there is a direct transition from O2$_S$ to C$_S$. The reverse transition (all closed states to O2$_S$, Fig. 11 A, $\triangle$) showed the same trend, indicating that opening to the O2$_S$ state occurred from the C$_S$ state more often than from the other closed states. The second clear connection was between the short-lived O1 state (O1$_S$) and an interme-

diate-length closed state (C$_M$). The adjacent state analysis (Fig. 11 B) showed that the highest proportion of O1$_S$ openings decayed to C$_M$ ($\bullet$). The reverse transition from the C$_M$ state to O1$_S$ ($\triangle$) was also more probable than opening to O1$_S$ from other closed states. However, there was also a significant fraction of transitions between O1$_S$ and C$_S$ ($\sim$30%, compared with 42% between O1$_S$ and C$_M$). When the percentages are this close, it is possible that both connections are direct. Alternatively, it could happen that all O1$_S$ events are directly connected to C$_S$, and go to C$_M$ only through a connection between C$_S$ and C$_M$. Since both C$_S$ and C$_M$ are closed states, the only way a C$_S$ event can be observed is when the channel immediately reopens. Otherwise, a closed time that falls into the exponential distribution of the C$_M$ state (e.g., 11.5 ms) cannot be distinguished from a closed time made up of combined C$_S$ and C$_M$ events [e.g., 1.5 ms (C$_S$) + 11.5 ms (C$_M$) + 2.0 ms (C$_S$), total closed time = 15 ms]. However, to observe more O1$_S$ events go to C$_M$ than to C$_S$, the rate between C$_S$ and C$_M$ must favor the C$_M$ transition over any reopening transition. If this were the case, we would expect to observe more O2$_S$ events decay to C$_M$. However, the graph in Fig. 11 A clearly shows that $\sim$90% of the O2$_S$ events were adjacent to C$_S$ events, meaning the rates for reopening must be higher than the rate to C$_M$. Therefore, we propose that both closed states (C$_S$ and C$_M$) can directly open to a single open state (O1$_S$). The

O3 state was less prominent; however, the data also suggested a connection between the $O3_S$ state and short closed states (not shown). For this analysis, we focused on connections between short-lived states. Connections between long-lived states are generally more difficult to determine since several short-lived states could occur in between.

To verify the simplified analysis described above, we then calculated two-dimensional component dependencies that compare the number of observed adjacent events to the number of expected adjacent events if the events occurred independently of each other (Magleby and Song, 1992; see MATERIALS AND METHODS). Table IV shows that the component dependencies support the connections deduced above. Independent pairing of states results in a component dependency = 0; positive numbers reflect the percentage of observations that were in excess of the expected number (i.e., 0.08 means 8% more adjacent events were observed than expected), and negative numbers are the percentage below the expected number of observations. Thus, positive numbers suggest a direct connection is likely between two states, and a negative number suggests a direct connection is unlikely. The numbers in the "data" columns suggest that there are direct connections between $O1_S$ and C_M, and between $O2_S$ and C_S. The value of 0.08 for $O1_S$ to C_S suggests a possible direct connection, but does not provide strong support. Conversely, direct connections from $O2_S$ to either C_M or C_L are not indicated. The apparent connection from $O1_S$ to C_L may arise from an indirect $O1_S$–C_M–C_L pathway, although we cannot rule out a direct connection.

A preliminary diagram that takes into account the number of observed states (see Table II) as well as the connections suggested by adjacent state analysis is shown in Scheme II (connections between the bracketed states are not yet determined).

$$\{C_{LLL} \quad C_{LL} \quad C_L\} \text{———} \quad C_M \text{—} C_S$$

$$O1_S \text{—} O2_S \text{—} O3_S$$

$$\{O1_L \quad O2_L \quad O3_L\}$$

(scheme ii)

As a first estimation, these connections appear to be consistent with the behavior observed in Fig. 1 for the doubly liganded channel. The most notable feature of the doubly liganded channel was that, although the overall open probability was very low, most openings occurred in bursts with short closings. This suggests that openings arise from short closed states or, put another way, that long closed states (C_L, C_{LL}, and C_{LLL}) do not directly give rise to open states. Furthermore, it implies that short closed states represent more highly acti-

table iv
Component Dependencies

	$O1_S$	$O2_S$	$O1_S$	$O2_S$
	data	*data*	*sim*	*sim*
C_S	0.080	1.602	0.603	1.152
C_M	2.173	−0.176	1.381	0.707
C_L	2.691	−0.624	1.416	0.646

This table supports the connections that were deduced from the dependency plots in Fig. 11. Positive numbers mean there is likely to be a direct connection, and negative numbers mean a direct connection is unlikely. Values >1 indicate the strongest connections, and states connected indirectly through intermediate closed states (C_M and C_L) have similar values. Calculations from the model (right) show the same trends as the data (left).

vated conformations than long closed states. Thus, close examination of bursting behavior seemed a good way to check our preliminary connections. First, we defined a burst as a group of consecutive events that contained at least 10 open events, and the only closed states within the burst could be classified as either C_M or C_S (the burst delimiter is the longest closed time allowed within the burst). This number of events was chosen to define a burst because there were three open and two closed states that we wanted to examine; 10 events seemed reasonable for all states to be represented. Results of the burst analysis are given in Table V. Interestingly, the mean number of openings per burst shows that all three open states (O1, O2, and O3) were accessible in the bursting state, as expected, but the O1 state was the predominant open state outside of bursts. This supports the notion that there might be two ways to open to O1: one in between bursts through

table v
Burst Statistics

	D	Mean No. of openings/burst O1	O2	O3	Mean burst closed time	Mean No. of openings/interburst O1	O2	O3
	ms				*ms ± SD*			
Two ligands	20	15	16	7	5.4 ± 2.7	11	1	0.05
Two ligands sim	20	6	4	1.4	4.5 ± 1.8	2.5	1.1	0.3
Three ligands	10	46	25	7	2.6 ± 0.9	1	0.2	0.02
Three ligands sim	10	45	44	9	1.69 ± 0.55	0.3	0.09	0
Two ligands	5	11	21	10	1.6 ± 0.6	25	3	0.2
Two ligands sim	5	4	4	2	1.71 ± 0.62	12	6	2
Three ligands	3	11	7	2	1.3 ± 0.4	5	1.6	0.09
Three ligands sim	3	8	9	2	1.04 ± 0.35	1.4	1.1	0.16

Events were from adjacent state analysis lists (see MATERIALS AND METHODS). Burst delimiter (D) is the longest closed time allowed inside the burst. Closed events longer than D were considered interburst intervals. The top half of the table uses burst delimiters that permit examining opening activity in the interburst intervals as well as within bursts. The bottom half uses burst delimiters that offer a closer look at openings that come directly from the shortest closed state (C_S).

C_M, and another during bursting through C_S. To test this idea further, the bursts were restricted to include mostly the shortest closed state (C_S), and open states were reexamined. Since the exponentials we have attributed to the shorter closed states (C_M and C_S) were somewhat overlapping (see Fig. 8), it was not possible to obtain a complete separation of C_M and C_S events. However, the average closed time within the burst (Table V) shows that the C_S state was in the majority. Upon inspection, all three open states occurred both before and after closing events within the burst, supporting the direct connections between C_S and all three open states. Moreover, O1 events also occurred outside the bursts. This suggests that opening in between bursts probably occurs most often from the C_M to the $O1_S$ state. Thus, the long interburst intervals appear to be transitions between long closed times that must pass through the C_M state before opening.

Similar connected-state and burst analyses were applied to data from triply liganded channels, and the same direct connections from the shortest closed state (C_S) to all three open states were observed. It is possible that what we are treating here as a single short closed state (C_S) is really several states with similar time constants, but a single C_S state is the most economical assumption.

Connections to long-lived openings are a bit more speculative. Long-lived openings were placed next to short openings of the same conductance, because transitions between short-lived openings of one conductance state and long-lived openings of another were sometimes observed without a closing between them. However, as discussed above, it is difficult to distinguish between transitions that enter long-lived states directly and transitions that enter a long-lived state by first passing through a short-lived state of the same conductance (e.g., $O1_S$–$O2_S$–$O2_L$). Nonetheless, the data suggest there might be direct, diagonal connections between the long-lived $O2_L$ and both the short-lived $O1_S$ and $O3_S$ states in doubly liganded channels. These connections appeared to change with liganding so that more ligands caused direct diagonal connections between $O1_S$ (and possibly $O2_S$) and $O3_L$.

Further refinements to the preliminary model were made from simulating a variety of different configurations. For these simulations, the rate constants were first put into a matrix format. The rate constants for each transition were calculated by using the relationship:

$$k_{si} = p_{si}\tau_s^{-1}; \qquad (\Sigma p_{si} = 1),$$

where k_{si} is the rate constant from state s to adjacent state i, p_{si} is the percent of total observed events from state s that go to a given adjacent state i, and τ is the lifetime of state s. Although there were five closed states measured in doubly liganded channels, only four closed states were used for simulations. This was reasonable, because the longest time constant was on the order of seconds, similar to the long closed times that were removed from the analysis by means of stability plots (see MATERIALS AND METHODS). The omission of this long-lived state did not significantly affect the opening behavior that was simulated in the doubly liganded model, although I/I_{max} was slightly higher than that measured from real data. To compare the properties of each configuration tested, the simulated data were analyzed in exactly the same way as the original data: single channel traces were inspected for their qualitative features, and amplitude and dwell-time histograms were constructed and fit. The overall configuration that best described all these aspects of the data at different levels of liganding is the connected state model shown in Fig. 9 A.

references

Biel, M., X. Zong, A. Ludwig, A. Sautter, and F. Hofmann. 1996. Molecular cloning and expression of a modulatory subunit of the cyclic nucleotide–gated cation channel. *J. Biol. Chem.* 271:6349–6355.

Bradley, J., J. Li, N. Davidson, H.A. Lester, and K. Zinn. 1994. Heteromeric olfactory cyclic nucleotide–gated channels: a subunit that confers increased sensitivity to cAMP. *Proc. Natl. Acad. Sci. USA.* 91:8890–8894.

Brown, R.L., W.V. Gerber, and J.W. Karpen. 1993. Specific labeling and permanent activation of the retinal rod cGMP-activated channel by the photoaffinity analog 8-*p*-azidophenacylthio-cGMP. *Proc. Natl. Acad. Sci. USA.* 90:5369–5373.

Brown, R.L., R. Gramling, R.J. Bert, and J.W. Karpen. 1995. Cyclic GMP contact points within the 63-kDa subunit and a 240-kDa associated protein of retinal rod cGMP-activated channels. *Biochemistry.* 34:8365–8370.

Brown, R.L., S.D. Snow, and T.L. Haley. 1998. Movement of gating machinery during the activation of rod cyclic nucleotide–gated channels. *Biophys. J.* 75:825–833.

Bucossi, G., M. Nizzari, and V. Torre. 1997. Single-channel proper-

ties of ionic channels gated by cyclic nucleotides. *Biophys. J.* 72:1165–1181.

Chen, T.-Y., Y.-W. Peng, R.S. Dhallan, B. Ahamed, R.R. Reed, and K.-W. Yau. 1993. A new subunit of the cyclic nucleotide–gated cation channel in retinal rods. *Nature.* 362:764–767.

Colquhoun, D., and A.G. Hawkes. 1995. The principles of the stochastic interpretation of ion-channel mechanisms. *In* Single-Channel Recording. 2nd edition. B. Sakmann and E. Neher, editors. Plenum Publishing Corp., New York. 397–482.

Colquhoun, D., and F.J. Sigworth. 1995. Fitting and statistical analysis of single-channel records. *In* Single-Channel Recording. 2nd edition. B. Sakmann and E. Neher, editors. Plenum Publishing Corp., New York. 483–587.

Cox, D.H., J. Cui, and R.W. Aldrich. 1997. Allosteric gating of a large conductance Ca-activated K$^+$ channel. *J. Gen. Physiol.* 110:257–281.

Dhallan, R.S., K.-W. Yau, K.A. Schrader, and R.R. Reed. 1990. Primary structure and functional expression of a cyclic nucleotide–activated channel from olfactory neurons. *Nature.* 347:184–187.

Eigen, M. 1968. New looks and outlooks on physical enzymology. *Q. Rev. Biophys.* 1:3–33.

Fesenko, E.E., S.S. Kolesnikov, and A.L. Lyubarsky. 1985. Induction by cyclic GMP of cationic conductance in plasma membrane of retinal rod outer segment. *Nature.* 313:310–313.

Finn, J.T., M.E. Grunwald, and K.-W. Yau. 1996. Cyclic nucleotide–gated ion channels: an extended family with diverse functions. *Annu. Rev. Physiol.* 58:395–426.

Gordon, S.E., M.D. Varnum, and W.N. Zagotta. 1997. Direct interaction between amino- and carboxyl-terminal domains of cyclic nucleotide–gated channels. *Neuron.* 19:431–441.

Gordon, S.E., and W.N. Zagotta. 1995a. Localization of regions affecting an allosteric transition in cyclic nucleotide–activated channels. *Neuron.* 14:857–864.

Gordon, S.E., and W.N. Zagotta. 1995b. Subunit interactions in co-ordination of Ni^{2+} in cyclic nucleotide–gated channels. *Proc. Natl. Acad. Sci. USA.* 92:10222–10226.

Goulding, E.H., J. Ngai, R.H. Kramer, S. Colicos, R. Axel, S.A. Siegelbaum, and A. Chess. 1992. Molecular cloning and single-channel properties of the cyclic nucleotide–gated channel from catfish olfactory neurons. *Neuron.* 8:45–58.

Goulding, E.H., G.R. Tibbs, D. Liu, and S.A. Siegelbaum. 1993. Role of H5 domain in determining pore diameter and ion permeation through cyclic nucleotide–gated channels. *Nature.* 364:61–64.

Goulding, E.H., G.R. Tibbs, and S.A. Siegelbaum. 1994. Molecular mechanism of cyclic-nucleotide–gated channel activation. *Nature.* 372:369–374.

Hackos, D.H., and J.I. Korenbrot. 1998. Selectivity for divalent cations changes as a function of ligand concentration in cGMP-gated channels of rod photoreceptors. *Biophys. J.* 74:A238. (Abstr.)

Hanke, W., N.J. Cook, and U.B. Kaupp. 1988. cGMP-dependent channel protein from photoreceptor membranes: single channel activity of the purified and reconstituted protein. *Proc. Natl. Acad. Sci. USA.* 85:94–98.

Haynes, L.W., A.R. Kay, and K.-W. Yau. 1986. Single cyclic GMP-activated channel activity in excised patches of rod outer segment membrane. *Nature.* 321:66–70.

Howe, J.R., S.G. Cull-Candy, and D. Colquhoun. 1991. Currents through single glutamate receptor channels in outside-out patches from rat cerebellar granule cells. *J. Physiol.* 432:143–202.

Ildefonse, M., and N. Bennett. 1991. Single-channel study of the cGMP-dependent conductance of retinal rods from incorporation of native vesicles into planar lipid bilayers. *J. Membr. Biol.* 123:133–147.

Karpen, J.W., and R.L. Brown. 1996. Covalent activation of retinal

rod cGMP-gated channels reveals a functional heterogeneity in the ligand binding sites. *J. Gen. Physiol.* 107:169–181.

Karpen, J.W., A.L. Zimmerman, L. Stryer, and D.A. Baylor. 1988. Gating kinetics of the cyclic-GMP–activated channel of retinal rods: flash photolysis and voltage-jump studies. *Proc. Natl. Acad. Sci. USA.* 85:1287–1291.

Kaupp, U.B., T. Niidome, T. Tanabe, S. Terada, W. Bönigk, W. Stühmer, N.J. Cook, K. Kangawa, H. Matsuo, T. Hirose, et al. 1989. Primary structure and functional expression from complementary DNA of the rod photoreceptor cyclic GMP-gated channel. *Nature.* 342:762–766.

Körschen, H.G., M. Illing, R. Seifert, F. Sesti, A. Williams, S. Gotzes, C. Colville, F. Müller, A. Dosé, M. Godde, et al. 1995. A 240 kDa protein represents the complete β subunit of the cyclic nucleotide–gated channel from rod photoreceptor. *Neuron.* 15:627–636.

Koshland, D.E., Jr., G. Nemethy, and D. Filmer. 1966. Comparison of experimental binding data and theoretical models in proteins containing subunits. *Biochemistry.* 5:365–385.

Liman, E.R., and L.B. Buck. 1994. A second subunit of the olfactory cyclic nucleotide–gated channel confers high sensitivity to cAMP. *Neuron.* 13:611–621.

Liu, D.T., G.R. Tibbs, P. Paoletti, and S.A. Siegelbaum. 1998. Constraining ligand-binding site stoichiometry suggests that a cyclic nucleotide–gated channel is composed of two functional dimers. *Neuron.* 21:235–248.

Liu, D.T., G.R. Tibbs, and S.A. Siegelbaum. 1996. Subunit stoichiometry of cyclic nucleotide–gated channels and effects of subunit order on channel function. *Neuron.* 16:983–990.

Liu, M., T.-Y. Chen, B. Ahamed, J. Li, and K.-W. Yau. 1994. Calcium-calmodulin modulation of the olfactory cyclic nucleotide–gated cation channel. *Science.* 266:1348–1354.

Magleby, K.L., and L. Song. 1992. Dependency plots suggest the kinetic structure of ion channels. *Proc. R. Soc. Lond. B Biol. Sci.* 249:133–142.

Matthews, G., and S.-I. Watanabe. 1988. Activation of single ion channels from toad retinal rod inner segments by cyclic GMP: concentration dependence. *J. Physiol.* 403:389–405.

Molokanova, E., B. Trivedi, A. Savchenko, and R.H. Kramer. 1997. Modulation of rod photoreceptor cyclic nucleotide–gated channels by tyrosine phosphorylation. *J. Neurosci.* 17:9068–9076.

Monod, J., J. Wyman, and J.-P. Changeux. 1965. On the nature of allosteric transitions: a plausible model. *J. Mol. Biol.* 12:88–118.

Nakamura, T., and G.H. Gold. 1987. A cyclic nucleotide–gated conductance in olfactory receptor cilia. *Nature.* 325:442–444.

Nakatani, K., and K.-W. Yau. 1988. Guanosine 3′,5′-cyclic monophosphate-activated conductance studied in a truncated rod outer segment of the toad. *J. Physiol.* 395:731–753.

Nizzari, M., F. Sesti, M.T. Giraudo, C. Virginio, A. Cattaneo, and V. Torre. 1993. Single-channel properties of cloned cGMP-activated channels from retinal rods. *Proc. R. Soc. Lond. B Biol. Sci.* 254:69–74.

Picco, C., C. Sanfilippo, P. Gavazzo, and A. Menini. 1996. Modulation by internal protons of native cyclic nucleotide–gated channels from retinal rods. *J. Gen. Physiol.* 108:265–276.

Picones, A., and J.I. Korenbrot. 1995. Spontaneous, ligand-independent activity of the cGMP-gated ion channels in cone photoreceptors of fish. *J. Physiol.* 485:699–714.

Root, M.J., and R. MacKinnon. 1994. Two identical noninteracting sites in an ion channel revealed by proton transfer. *Science.* 265:1852–1856.

Rosenmund, C., Y. Stern-Bach, and C.F. Stevens. 1998. The tetrameric structure of a glutamate receptor channel. *Science.* 280:1596–1599.

Rothberg, B.S., R.A. Bello, and K.L. Magleby. 1997. Two-dimensional components and hidden dependencies provide insight into ion channel gating mechanisms. *Biophys. J.* 72:2524–2544.

Ruiz, ML., R.L. Brown, Y. He, T.L. Haley, and J.W. Karpen. 1999. The single channel dose–response relation is consistently steep for rod cyclic nucleotide–gated channels. *Biophys. J.* 76:A8. (Abstr.)

Ruiz, ML., and J.W. Karpen. 1997. Single cyclic nucleotide–gated channels locked in different ligand-bound states. *Nature.* 389: 389–392.

Sigworth, F.J., and S.M. Sine. 1987. Data transformations for improved display and fitting of single-channel dwell time histograms. *Biophys. J.* 52:1047–1054.

Tanaka, J.C. 1993. The effects of protons on 3′, 5′-cGMP–activated currents in photoreceptor patches. *Biophys. J.* 65:2517–2523.

Taylor, W.R., and D.A. Baylor. 1995. Conductance and kinetics of single cGMP-activated channels in salamander rod outer segments. *J. Physiol.* 483:567–582.

Tibbs, G.R., E.H. Goulding, and S.A. Siegelbaum. 1997. Allosteric activation and tuning of ligand efficacy in cyclic-nucleotide–gated channels. *Nature.* 386:612–615.

Varnum, M.D., K.D. Black, and W.N. Zagotta. 1995. Molecular mechanism for ligand discrimination of cyclic nucleotide–gated channels. *Neuron.* 15:619–625.

Varnum, M.D., and W.N. Zagotta. 1996. Subunit interactions in the activation of cyclic nucleotide–gated ion channels. *Biophys. J.* 70: 2667–2679.

Varnum, M.D., and W.N. Zagotta. 1997. Interdomain interactions underlying activation of cyclic nucleotide–gated channels. *Science.* 278:110–113.

Zagotta, W.N., T. Hoshi, and R.W. Aldrich. 1994. *Shaker* potassium channel gating. III: Evaluation of kinetic models for activation. *J. Gen. Physiol.* 103:321–362.

Zimmerman, A.L. 1995. Cyclic nucleotide–gated channels. *Curr. Opin. Neurobiol.* 5:296–303.

Zimmerman, A.L., and D.A. Baylor. 1986. Cyclic GMP-sensitive conductance of retinal rods consists of aqueous pores. *Nature.* 321: 70–72.

Zong, X., H. Zucker, F. Hofmann, and M. Biel. 1998. Three amino acids in the C-linker are major determinants of gating in cyclic nucleotide–gated channels. *EMBO (Eur. Mol. Biol. Organ.) J.* 17: 353–362.